TWELVE

JLab Program Advisory Committee ~~Eleven~~ Proposal Cover Sheet

This document must be received by close of business on ~~Wednesday, December 18, 1996~~ JUNE 26 1997 at:

Jefferson Lab
User Liaison Office, Mail Stop 12 B
12000 Jefferson Avenue
Newport News, VA 23606

(Choose one)

☐ **New Proposal Title:** Electroproduction of the $pp\pi^-$ System off the Deuteron Beyond the Quasifree Region

☐ **Update Experiment Number:**

☐ **Letter-of-Intent Title:**

Contact Person

Name: Nikolai A. Pivnyuk, Leonid S. Vorobyev
Institution: ITEP
Address: Bolshaya Cheremushkinskaya 25
Address:
City, State ZIP/Country: 117259, Moscow, Russia
Phone: 7-(095)-125-9542 **FAX:** 7-(095)-123-6584
E-Mail › Internet: pivnyuk@cebaf.gov

Experimental Hall: B **Days Requested for Approval:** 16

Jefferson Lab Use Only

Receipt Date: 6/23/97 PR 97-001

By: go

BEAM REQUIREMENTS LIST

Lab Proposal No.: _____ Date: _____

Hall: _____ Anticipated Run Date: _____ PAC Approved Days: _____

Spokesperson: Nikolai A. Pivnyuk
Phone: 7-(095)-125-9242
E-mail: Pivnyuk@cebaf.gov

Hall Liaison: _____

List all combinations of anticipated targets and beam conditions required to execute the experiment. (This list will form the primary basis for the Radiation Safety Assesment Document (RSAD) calculations that must be performed for each experiment.)

Condition No.	Beam Energy (MeV)	Mean Beam Current (μA)	Polarization and Other Special Requirements (e.g., time structure)	Target Material (use multiple rows for complex targets — e.g., w/windows)	Material Thickness (mg/cm²)	Est. Beam-On Time for Cond. No. (hours)
1	4000	30 nA	none	standard liquid deuterium target		

The beam energies, E_{Beam}, available are: $E_{Beam} = N \times E_{Linac}$ where N = 1, 2, 3, 4, or 5. E_{Linac} = 800 MeV, i.e., available E_{Beam} are 800, 1600, 2400, 3200, and 4000 MeV. Other energies should be arranged with the Hall Leader before listing.

HAZARD IDENTIFICATION CHECKLIST

JLab Proposal No.: _____ Date: _____
(For CEBAF User Liaison Office use only.)

Check all items for which there is an anticipated need.

Cryogenics
_____ beamline magnets
_____ analysis magnets
_____ target
type: _____
flow rate: _____
capacity: _____
none unique to this experiment

Electrical Equipment
_____ cryo/electrical devices
_____ capacitor banks
_____ high voltage
_____ exposed equipment
none unique to this experiment

Radioactive/Hazardous Materials
List any radioactive or hazadorous/ toxic materials planned for use:
_____
none
_____
_____

Pressure Vessels
_____ inside diameter
_____ operating pressure
_____ window material
_____ window thickness
none unique to this experiment

Flammable Gas or Liquids
type: _____
flow rate: _____
capacity: _____

Drift Chambers
type: argon/ethane
flow rate: _____
capacity: _____

Other Target Materials
___ Beryllium (Be)
___ Lithium (Li)
___ Mercury (Hg)
___ Lead (Pb)
___ Tungsten (W)
___ Uranium (U)
___ Other (list below)
_____
none

Vacuum Vessels
_____ inside diameter
_____ operating pressure
_____ window material
_____ window thickness
none unique to this experiment

Radioactive Sources
_____ permanent installation
_____ temporary use
type: _____
strength: none

Large Mech. Structure/System
_____ lifting devices
_____ motion controllers
_____ scaffolding or
_____ elevated platforms
none unique to this experiment

Lasers
type: none
wattage: _____
class: _____

Installation:
_____ permanent
_____ temporary

Use:
_____ calibration
_____ alignment

Hazardous Materials
____ cyanide plating materials
____ scintillation oil (from)
____ PCBs
____ methane
____ TMAE
____ TEA
____ photographic developers
____ other (list below)
_____
_____
none

General:

Experiment Class:

_X_ Base Equipment
_____ Temp. Mod. to Base Equip.
_____ Permanent Mod. to Base Equipment
_____ Major New Apparatus

Other: _____
_____

Draft, 17–March–1997

Electroproduction of the $pp\pi^-$ System off the Deuteron Beyond the Quasifree Region

Spokespersons: N. Pivnyuk,

L. Vorobyev

S. Boyarinov, P. Degtyarenko, M. Kossov, G. Leksin, B. Martemyanov, K. Mikhailov, N. Pivnyuk, O. Pogorelko, P. Ryzhak, M. Schepkin, V. Serov, A. Stavinsky, A. Vlassov, L. Vorobyev

Institute for Theoretical and Experimental Physics, Moscow, Russia

V. Kolybasov

Lebedev Physical Institute, Moscow, Russia

W. Brooks, V. Burkert, D. Cords, D. Heddle, B. Mecking, E. Smith, E. Wolin

Thomas Jefferson National Accelerator Facility, Newport News, Virginia, USA

D. Heddle

Christopher Newport University, Newport News, Virginia, USA

J.R. Calarco, W. Hersman, T.P. Smith

University of New Hampshire, Durham, NH, USA

H.A. Clement, G.J. Wagner

Physikalisches Institut der Universität Tübingen, Germany

The Proposal is open for collaboration

Abstract

The proposed research aims at the experimental investigation of the exclusive reaction $ed \to e'pp\pi^-$ not far above threshold, as well as in Δ–region, and at momentum transfer $Q^2 \geq 1$ GeV^2. In this kinematical region the reaction is known to be extremely sensitive to short–range correlations in the deuteron. Estimates of the reaction cross section are given, and the feasibility of the proposed research is considered. The CLAS detector at *CEBAF* appears to be well suited for measurements of the $pp\pi^-$ electroproduction off the deuteron.

Introduction.

We propose a detailed experimental investigation of the $ed \to e'pp\pi^-$ reaction in the kinematical region far from the conventional quasifree region, that is, in the region where the contribution of quasifree mechanism of π^--production is highly suppressed. In particular, we propose to perform the experimental measurements :

- at $Q^2 > 1$ GeV^2,
- at $\Delta M = M_{pp\pi^-} - (m_p + m_p + m_{\pi^-}) < 600$ MeV,
- with constraints on proton momenta $p_p > 300$ MeV/c.

The CEBAF CLAS detector fits these conditions perfectly for experimental measurements of the $ed \to e'\ pp\pi^-$ reaction with four charged particles in the final state.

The kinematical region for the proposed experiment is interesting from different points of view, and its investigation will provide important information for both particle and nuclear physics. The main motivation for this experiment is, of course, the following: **the short distances in the deuteron will contribute significantly to the cross section with the kinematical constraints outlined above** [1,2].

The main issues of the proposed experiment are :

– Exclusive measurements of the reaction $ed \to e'pp\pi^-$ will permit study of the "simplest" reaction mechanisms when the **proton momenta are large** ($p > 300 MeV/c$) **compared to the typical momentum of a nucleon in the deuteron** ($p < 100 \div 150 MeV/c$). This is due to the specific dynamical features of the pole graph, Fig. 1,a and of the triangle graphs (with e.g. pp rescattering in the final state, Fig. 1,b). This could allow in turn to draw conclusions about the possible **contribution of more exotic states in the deuteron** (short-range correlations, $6q$ states, $\Delta\Delta$ admixture in deuteron, etc.).

– Detailed investigation of the pp final state interaction (FSI) in a wide range of Q^2 and $M_{pp\pi^-}$. It will provide information about the **size of the proton emission source** in this reaction, and about the dynamics of the reaction which mainly relies on the short distances in the deuteron.

– Detailed investigation of the $p\pi^-$ invariant mass distribution will allow to study the contribution and the dynamical features of the diagrams with Δ-isobar in intermediate and final states. Valuable experimental information could be obtained for understanding the **influence of the nuclear medium on the dynamical features of Δ-isobar production in nuclei.**

– Detailed investigation of the $pp\pi^-$ invariant mass distribution in the region close to the threshold of π^--production off the deuteron will make it possible **to clarify the situation with regard to the existence of a narrow NN-decoupled dibaryon resonance** that has been proposed [3] to explain specific peculiarities observed in hadronic reactions [4,5].

– Detailed investigation of the $pp\pi^-$–system in the kinematical region close to the Δ–region ($\Delta M > 200$ MeV) will **test theoretical predictions** [6] **which concern basic and specific features of the triangle diagrams.**

We also hope that these measurements will provide new, independent, and complementary information to that from the experimental investigations which are already planned at CEBAF: experimental investigations of the deuteron disintegration at threshold, Hall

A [7], Δ-production off nuclei, Hall B [8], and Δ-Δ component in the deuteron, Hall B [9].

Kinematical region and the method of extraction of the reaction $ed \to e'pp\pi^-$.

In the following sections we will concentrate on the deuteron as a target. Shown in Fig. 2 is the momentum transfer squared, Q^2, versus the mass difference $\Delta M = M_{pp\pi^-} - (M_d + m_\pi)$. In terms of these variables, the invariant mass of a system produced on a single isolated nucleon in the deuteron increases with Q^2 if the second nucleon stays at rest. As an example, we show two specific "trajectories". The first one corresponds to the threshold π^--production on the deuteron, and the second to the Δ-production threshold. Both curves correspond to the quasifree mechanism, where the nucleon-spectator is considered being at rest.

The vertical line corresponds to the production of the $pp\pi^-$–system on the deuteron as a whole. The vertical trajectory in this picture corresponds to the threshold for Δ-production on the deuteron as a whole, $M_{pp\pi^-} = M_N + M_\Delta$, when the relative momentum of N and Δ equals zero.

As is seen from Fig. 2, for larger values of Q^2 the distance between the trajectories for quasifree production on one of the nucleons, and any vertical trajectory corresponding to $NN\pi$–production on the deuteron as a whole is increasing. In other words, **the role of quasifree π^-–production gets weaker as Q^2 increases.**

Another independent way to suppress quasifree interaction would be to cut off events with proton momenta $\sim 50 \div 150$ MeV/c typical for the spectator mechanism. **We suggest studying the $ed \to e'pp\pi^-$ reaction with constraints on proton momenta $P_p > 300$ MeV/c.**

At small invariant masses these two ways are equivalent. However, for the values of $M_{pp\pi^-}$ typical for quasifree trajectories the second way, the P_p cut–off, is unique.

The momentum threshold for proton detection by the CLAS set up at full magnetic field, $B/B_0 = 1$, is ~ 300 MeV/c. Thus the second way to suppress the quasifree mechanism is provided automatically for the CLAS detector. If necessary, this way to suppress the quasifree contribution could be made even more severe in the off-line data analysis.

At the same time, it would also be interesting to trace the behavior of the cross section for softer constraints on spectator's momentum, $P_p > (150 - 200)$ MeV/c. It would be possible due to the planned runs for the CLAS setup with a weaker magnetic field, $B/B_0 = 1/2$.

For the event selection in the region $\Delta M \leq 100$ MeV, where the pion momentum mostly will not be sufficient to hit all three regions of CLAS Drift Chamber and TOF counters, see Fig. 3, we will use the missing mass method for pion identification. As a matter of fact, all soft ($P_{\pi^-} \sim 150 \div 200$ MeV/c) charged pions hit *at least* two or three superlayers of the drift chambers, Fig. 3. Thus this "additional" information about the missing particle's trajectory will allow to perform a more accurate missing mass analysis in the kinematical region $\Delta M \leq 100$ MeV.

Cross sections of the reaction $ed \to e'X$, available at present. Lower limit of the $ed \to e'pp\pi^-$ reaction cross section. The expected statistics.

At present, there are no data on the exclusive reaction $ed \to e'pp\pi^-$ for $Q^2 > 0.5$ GeV^2 and $M_{pp\pi^-} < 3$ GeV. Shown in Fig. 4,a,b,c are the experimental data on the reaction $ed \to e'X$ from Ref.[10] (dots), recalculated for the initial energy $E_0 = 4$ GeV, and $Q^2 = 1.0$ (a), 1.5 (b), and 2.0 GeV^2, (c), respectively. It is assumed that in this kinematical region ($\Delta M > 200$ MeV) the $pp\pi^-$-channel contributes $\sim 30\%$.

The experimental data [10] which were used for our estimates of the cross section are in good agreement with another independent experimental result obtained for the reaction $ep \to e'X$ at $E_0 = 4.88$ GeV, [11].

Shown in Fig. 4 is the cross section $d^2\sigma/d\nu dQ^2$ in pb/(MeV GeV^2). The solid curves are theoretical predictions based on the pole diagram normalized to the experimental data in the Δ-region. As can be seen, the ΔM-dependence is well described by the calculations at $\Delta M \sim 300 - 400$ MeV.

Theoretical estimates at $Q^2 = 1 \div 2$ GeV^2 and $\Delta M < 100$ MeV with the Paris deuteron wave function [12] lead to ~ 2 orders of magnitude smaller cross section $d^2\sigma/dQ^2d\nu$ as compared to the estimates obtained from the extrapolation described above, and shown in Fig. 4,a,b,c. As already pointed out, at small ΔM the main contribution is due to the diagrams that do not vanish in the limit of small 4-momentum of π^--meson in the $pp\pi^-$ rest frame. Numerically the main contribution is due to the contact Kroll–Ruderman term (the so called "seagull" term) enhanced by pp final state interaction. It is known that this contribution can be written in a gauge invariant way. Let us stress that at small Q^2 the same formulae lead to the value of the cross section which agrees very favorably with the SACLAY experimental data at $Q^2 \sim 0.1$ GeV^2, and which are in agreement with the recent theoretical calculations given in Ref.[13].

The region of $Q^2 > 1$ GeV^2 is known to be sensitive to the short-range (e.g. 6q) component in the deuteron if ΔM is small enough. Indeed, our estimates of the 6q–contribution show that it exceeds the contribution of the "conventional" np–component of the deuteron calculated with the Paris potential by two orders of magnitude at $\Delta M \sim 50$ MeV and $Q^2 = 1 \div 2$ GeV^2. These estimates are model dependent. We assumed that in the static limit the 6q–admixture in the deuteron is of the order of $1 \div 2\%$, and that the transition formfactor in the vertex $\gamma^*(6q)_d \to pp\pi^-$ behaves like the elastic 6q–formfactor of the deuteron (see, e.g. [14]). The estimated values of the cross section at $\Delta M = 20 \div 80$ MeV are :

1.5×10^{-3} pb/MeV·GeV^2 at $Q^2 = 1.0$ GeV^2,
1.7×10^{-4} pb/MeV·GeV^2 at $Q^2 = 1.5$ GeV^2,
2.8×10^{-5} pb/MeV·GeV^2 at $Q^2 = 2.0$ GeV^2.

As can be seen, these theoretical estimates for the possible $6q$–state contribution to the cross section are of the **same order of magnitude** as our expectations for the quasifree contribution based on the experimental results [10,11], see Fig. 4,a,b,c.

Predictions of the pole mechanism (Fig. 1,a) for the reaction $ed \to e'pp\pi^-$ with the cuts on proton momentum, $P_p > 300$ MeV/c, are shown by the dashed curves in Fig. 4,a-c for different values of momentum transfer. Our estimates at small ΔM make it possible

to compare the Q^2–dependence of the cross section near threshold with the similar dependence of the deuteron disintegration cross section measured at Saclay (see e.g. [15]) not far above np–threshold. These curves have very similar slopes, see Fig. 5.

Based on these predictions, the lower limit for the expected number of events is given in Fig. 6 as a function of the $pp\pi^-$ invariant mass for three intervals of Q^2: (0.75 – 1.25), (1.25 – 1.75), and (1.75 – 2.25) GeV^2, and with the ΔM–interval = 25 MeV. These estimates were made for a luminosity $L = 10^{34} cm^{-2} sec^{-1}$, acceptance 0.75, and a run time of 400 hours.

From Fig. 6, it is seen that the expected statistical accuracy will make it possible to perform partial wave analysis for the system $pp\pi^-$ at least for $\Delta M >\sim 100$ MeV, and for $Q^2 = (0.75 - 2.5)$ GeV^2. For $\Delta M \sim (40 - 100)$ MeV such an analysis is feasible for $Q^2 = (0.75 - 1.5)$ GeV^2.

Reaction mechanisms below and in the Δ–resonance region.

The mechanism of π^--electroproduction off nuclei in general (and off the deuteron in particular) in the kinematical region far from the conventional quasifree domain, and at high Q^2, has not been studied experimentally or theoretically.

It's quite natural to expect that a significant role in the process will be played by non–conventional (exotic) components of the deuteron wave function (short-range correlations or in other words "long tails" in Fermi distribution, admixtures of $6q$ states and Δ-Δ component in the deuteron, etc).

To distinguish between different mechanisms in the future analysis of the data and to draw conclusions about the "exotic" contribution to the cross section we should extract the contributions of the "simplest" graphs (see Fig. 1a,b). For example, below the Δ–region , $\Delta M < 100$ MeV, diagrams in Fig. 1,b should contribute significantly. At larger invariant masses for the $pp\pi^-$ system, $\Delta M \sim 200 - 600$ MeV, the graphs with a Δ isobar in the final, Fig. 7, and intermediate, Fig. 8, states could constitute the major part of the cross section. To distinguish between different reaction mechanisms one should take into account all specific dynamical features and criteria for the different mechanisms.

The main, "model independent", and pronounced feature of any pole graph is that the upper and lower vertices are practically independent. This peculiarity is strengthened with increasing Q^2. For that reason, one could expect significant differences in momentum and angular distributions of the secondaries produced due to the pole and triangle mechanisms. Preliminary calculations made for the pole graph and triangle graph with pp-rescattering in the final state confirm these expectations. Consider first a single event. In each event one of the two detected protons has momentum larger than the other proton. Let it be the "fast" proton, and the other, respectively, the "slow" proton. Fig. 9 demonstrates how simple kinematical constraints based on the combined consideration of the "fast" and "slow" proton momenta, could provide in the future simple event selection tools for the suppression of the contribution of either the pole graph, Fig. 1a, ($D > -150$. cut on Fig. 9c) or triangle graph, Fig. 1b, ($D < -350$ cut on Fig. 9d). If we consider the combination of the "fast" proton momentum and pion momentum (see Fig. 10) we will obtain additional possibilities for the separation of the contributions of the pole and triangle graphs. An example would be a cut such as $D < -100$ on Fig. 10c,d.

The features discussed suggest a unique tool to distinguish between these diagrams, and **ultimately to investigate contributions of the short range correlations in the deuteron**. Let us note that the contribution of the triangle graph (Fig. 1b) should dominate at small invariant masses of the $pp\pi^-$–system, and should lead to the pp–invariant mass distribution peaked at small values of M_{pp} (the well known Migdal–Watson effect of the FSI).

There are some specific features of the triangle diagrams predicted by the standard theory which have not yet been investigated experimentally. A distinct qualitative indication of the triangle mechanism has been known for many years[6]. This is the so called moving complex singularity: the triangle graph of Fig. 11 has a singularity of the logarithmic type as a function of the variable W – invariant mass of n particles produced at the right lower vertex of the triangle. Its position in the complex plane depends on the value of the variable q – the total momentum of these n particles, see Fig. 11. Therefore the position and width of the bump in the W–distribution must vary with q. The experimental observation of this predicted feature would give evidence for the dominance of the triangle graph shown in Fig. 11. For our reaction it might unambiguously manifest itself in the channel with the Δ isobar in the intermediate state at $\Delta M \approx 100 - 200$ MeV, see Fig. 8a. It would be highly desirable to test these predictions experimentally.

It is quite natural to expect that in the kinematical domain $\Delta M > 100$ MeV π^- production is mainly due to the Δ isobar (Fig. 7,8) in the intermediate states. Fig. 7b points to an interesting mechanism of the reaction. Pion rescattering on the spectator proton increases the spectator momentum, and so this diagram contributes to our kinematical domain. At the same time, this $\pi^- p_s$–rescattering will result in a distortion of the Δ-isobar peak. Estimates made under the assumptions that the average pion momentum before rescattering is about 250-300 MeV/c, and rescattering takes place on the proton spectator at rest, show that one will observe the Δ-isobar peak shifted down to values of 1080 – 1130 MeV with a width in the order of 130 – 160 MeV, which is larger than the vacuum width of the Δ–isobar. Undoubtedly, it would be quite important to test the validity of this prediction in the experiment.

Such experimental data could contribute significantly to our understanding of the process of Δ-isobar production off nuclei which is planned to be investigated at CEBAF [8].

Investigation of the pp and $pp\pi^-$ invariant mass spectra. Partial wave analysis.

As was pointed out, at small $M_{pp\pi^-}$–masses the reaction mechanism is very sensitive to short-range correlations in the deuteron if Q^2 is not small, $Q^2 = 1 \div 2$ GeV^2. It is also clear that s–wave production (all the three particles are in relative s-state) dominates near threshold. In such a situation the singlet virtual state ($^1S_0$) in the pp–subsystem plays a crucial role. As is well known, the pp final state interaction (Fig. 1,b) becomes stronger as the size of interaction region gets smaller. This situation is ideally realized in the kinematical region considered here. At $\Delta M \leq 100$ MeV the diagram with pp–rescattering enhances any reaction mechanism of s–wave production by an order of magnitude. The enhancement factor rises as the $pp\pi^-$–invariant mass approaches threshold. It would be

interesting to trace the behavior of s–wave production and the variation of the size of the interaction region as the $pp\pi^-$–invariant mass increases, and Q^2 varies within the interval $Q^2 \sim 0.75 \div 2.5$ GeV^2. As is demonstrated in Fig. 6, such an analysis is feasible with the expected statistics. The pp–invariant mass distributions for different reaction mechanisms (Fig. 1,a and b) are shown in Fig. 12a and b, respectively. Shown in Fig. 12c, d are correlation functions, obtained by dividing the M_{pp}–distributions in Fig. 12a, b by the corresponding M_{pp} phase space distribution.

One of the goals of the proposed research is the **investigation of the $pp\pi^-$ invariant mass spectrum in order to search for narrow structures with quantum numbers forbidden in NN–system.**

As already mentioned, the $pp\pi^-$–system produced in $\gamma^* d$–reaction near threshold preferably has quantum numbers $J^P = 0^-$, and $T = 1$ or 0, the latter being forbidden in the NN-system by the Pauli exclusion principle. Exactly these quantum numbers are carried by the lightest $6q$–state that decouples from NN [3], this qualitative statement being independent of any particular model parameters.

Although resonances in the dibaryon system have been predicted long ago on the basis of QCD-inspired models, no unambiguous evidence for their existence has been found despite a large number of dedicated experiments [17]. However, most of these searches aimed at NN–coupled resonances, the decay of which is expected to result in large widths, making them practically indistinguishable from non-resonant processes. For the first time very recently a candidate for a narrow NN-decoupled resonance NNπ (called d' henceforth) has been detected in different reactions and different experiments which specifically focus onto the πNN system and small NN–distances. The singularity of the $pp\pi^-$ mass spectrum observed in the elementary reaction, $pp \to pp\pi^-\pi^+$ [4], the resonant–like behavior of the excitation function in low energy pionic double charge exchange (DCX), π^+(A,Z) $\to$ (A,Z+2)π^- at $T_\pi \sim 50$ MeV, and the peculiar shape of the DCX cross section on ^4He at $T_\pi \sim 100$ MeV [5], can be naturally explained by the signature of the d' resonance with a mass of $M_{d'} \approx 2.06$ GeV (for more details see the Appendix, and Figs. 13, 14). The very small $NN\pi$ decay width of d', $\Gamma_{NN\pi} \approx 0.5$ MeV, deduced from DCX experiments, appears to be quite reasonable, since the energy release in the NNπ–decay is small (the d' mass is only ~ 50 MeV above NNπ-threshold), see also [18].

Though the strong decay of d' into NN is forbidden by its quantum numbers, its formation or production relies on two closely spaced nucleons. Hence d' production (or formation) by real or virtual γ might be possible in a situation where one deals with a spatially strongly correlated np–pair.

The most elementary reaction for d' production would be, in principle, the reaction $\gamma d \to d' \to NN\pi$ where the d' can manifest itself as a Breit–Wigner pole at $\omega_\gamma \sim 200$ MeV. However, conventional charged pion photoproduction on the deuteron in this energy range could mask any d'–signal completely.

As already discussed, at high Q^2 any reaction mechanism of $pp\pi^-$–electroproduction of the deuteron is very sensitive to short–range correlations in the deuteron, in particular for small $pp\pi^-$–invariant masses. In other words, π–electroproduction is confined to the interaction of γ^* with the $6q$–component in the deuteron. Thus we expect that the "signal to background" ratio should improve drastically, if the d' is produced by virtual γ^* with large Q^2.

In Ref.[19] the $d' \to d\gamma$ decay rate was estimated using d'–parameters deduced from pionic DCX, $\Gamma(d' \to d\gamma) \sim 0.1$ keV. It is straightforward now to estimate the cross section of resonant pion photoproduction on the deuteron, $\gamma d \to d' \to pp\pi^-$ at $\omega_\gamma \sim 200$ MeV. For $\Gamma_{\gamma d} \sim 0.1$ keV we obtain $\sigma_{res} \sim 1$ μb, which is very small compared to the known cross section ($\sigma_{nr} \simeq 150\mu b$) [11,20] for charged pion photoproduction at this energy. This renders the search for the d'–signal extremely difficult.

The contribution of the $6q$–component of the deuteron to the pion photoproduction is of the order $P_{6q} \cdot \sigma_{nr}$. For $P_{6q} \sim 1\%$ this contribution is comparable or even smaller than σ_{res}. Therefore it seems reasonable to expect that the d' contribution to charged pion electroproduction dominates in regions of the momentum transfer where the nonresonant pion production is mainly due to the $6q$–component of the deuteron, and also spectator mechanisms are suppressed. Estimates of such Q^2 as well as estimates of $6q$–contribution to the deuteron formfactors are ambiguous [14,19]. We think that at intermediate Q^2 (e.g. $Q^2 > 1 - 2GeV^2$) the situation might be most favorable.

The process $ed \to e'd'$ is described by the amplitude proportional to the transition 6q–formfactor corresponding to d' formation by virtual γ^* on $6q$–component of the deuteron. The estimated value of the cross section for d' electroproduction on the deuteron and the corresponding number of events (ΔN) of the reaction $ed \to e'd' \to e'pp\pi^-$ for different values of Q^2 are given in the Table 1. For comparison the number of background events (Δn) estimated from Fig. 6 are also presented in Table 1. Both ΔN and Δn were estimated under the same assumptions: the luminosity $L = 10^{34} cm^{-2} sec^{-1}$, an acceptance of 0.75, and a run time of 400 hours.

For more details concerning the CLAS acceptance and invariant mass resolution see the Appendix.

Table 1

Q^2	$d^2\sigma/dQ^2$	$\Delta N/0.5$ GeV^2	$\Delta n/0.5$ GeV^2/5 MeV
GeV^2	pb/GeV^2	1/GeV^2	1/GeV^{2}MeV
1.0	0.330	1780	140
1.5	0.050	0270	1.5
2.0	0.013	0070	0.2
2.5	0.003	0018	—

From the arguments given above we expect that the competing nonresonant pion production will not be much larger than the d' electroproduction. There are also some additional possibilities to significantly improve the signal to background ratio due to the proper event selection in future analysis. It can be possible mainly due to the specific behaviour of the pp invariant mass distribution for the d' decay. See the Appendix for

more detail concerning two body invariant mass distributions either for the d' decay or for the continuum.

The expected numbers of events presented in Table 1 are estimated for the already approved run time (400 hours) and only for the deuterium target. It is quite natural to expect that we will obtain much better statistics for the analysis of future runs on light nuclear targets such as ^3He. It should be pointed out that investigation of π^- production near the threshold on light nuclei could turn out to be extremely interesting not only as an additional opportunity to obtain better statistics but rather as a unique chance to get a better understanding of the nature of the expected effect. If the spike in the $pp\pi^-$–invariant mass distribution will be found on the deuterium target than only detailed investigations of the same effect on the lightest nuclei could provide a chance to distinguish between two hypotheses – does the observed effect result from the strong final state interaction in the $pp\pi^-$ system, or are we observing d' resonance production. For more details concerning these points see the Appendix.

Appendix

The CLAS Acceptance and Invariant Mass Resolution.

Calculations of acceptance and $pp\pi^-$ invariant mass resolution for different types of events were done by means of Monte–Carlo (MC) simulations. The SDA program for simulation and reconstruction of different events of $eX \to e'X'$ reactions was used.

It should be pointed out that the suggested experiment focuses onto the investigation of rather small invariant masses of the $NN\pi$ system. Thus during the acceptance calculations one has to make sure that none of pairs of particles can hit one and the same wire or two neighbouring wires in the DC region. It is clear that the most "dangerous" one is the DC region 1 – the closest to the target. Therefore during the course of the event reconstruction only those events which were supposed to be really detected for which any pair of particles satisfied the condition $\Delta\theta = \theta_1 - \theta_2 > 4^0$, where θ_1 and θ_2 – polar angles of particle tracks. This cut reduces the expected acceptance by 30 – 40%. Note that the problem of pattern recognition for close tracks is quite important for a number of reactions, and in particular for those where one has to deal with small relative momenta of particles.

For the events with slow π^-, which is quite typical for the reaction considered (see, e.g. track 2 in Fig.3), the π^-–momentum determination was done via the missing mass analysis, i.e., only using the information about the momenta of the protons and outgoing electron (see acceptance on Fig.15,a and resolution on Fig.16,a).

The π^- reconstruction when the π^- hits the DC Region 1 and the π^- hits DC Regions 1 and 2 was done taking into consideration the information from DC. The corresponding acceptance and invariant mass resolution are presented on Fig.15,b and Fig.16,b (π^- hits DC Region 1) and Fig.15,c and Fig.16,c (π^- hits DC Regions 1 and 2). The values of the acceptance and mass resolution for the case of the event reconstruction when all the DC and TOF information is available are presented on Fig.15,d and Fig.16,d.

These preliminary calculations demonstrat that the accurate momentum reconstruction for soft pions which hit only two regions of the CLAS Drift Chamber is absolutely feasable and will reach the same accuracy in the invariant mass reconstruction as for events when the π^- hits all DC regions and TOF counters.

Figures 15 and 16 demonstrate the acceptance and the invariant mass resolution for different types of events. The detailed calculations show a weak Q^2–dependence of the acceptance and invariant mass resolution when Q^2 ranges between 1 and 3 GeV^2. The invariant mass resolution shown in Fig.16 was obtained for the interval $M_{pp\pi^-} < 2.2$ GeV.

First Results from the ITEP Experiment on the Two Pion Production in pp Collisions. Strong pp FSI. Two and Three Body Invariant Mass Distributions in the $pp\pi^-$ System.

The most elementary reaction to search for the d' resonance in hadronic collisions is $pp \to d'\pi^+ \to pp\pi^-\pi^+$.

At ITEP the reaction $pp \to pp\pi^-\pi^+$ has recently been measured at $T_p = 900$ MeV using a plastic-like wall set-up. For the first time the emphasis was put onto the investigation of the $pp\pi^-$ and $pp\pi^+$ mass spectra [4].

If the spin and parity of the $pp\pi$ system are $J^P = 0^-$, the two protons are preferably in a relative S–wave. In that case there should be strong effects from the pp final state interaction: essential enhancement of the number of events with a small invariant mass in the pp subsystem. The same effect leads to a dominance of the triangle graph (Fig. 5b) in non-resonant $pp\pi^-$ electroproduction not far above threshold. Note that the FSI affects the $p\pi^-$ invariant mass spectrum as well, thus for the d' events the pp and $p\pi^-$ mass spectra must be correlated. The predicted distributions $d\Gamma/dM_{pp}$ and $d\Gamma/dM_{p\pi}$ in the $pp\pi^-$-decay of the d' resonance are given in Fig.17. For more detail see Ref.[18]. The M_{pp} mass spectrum allows to selectively look for the d' signal in the $pp\pi$-mass spectrum by constraining the pp-invariant mass, $M_{pp} < 2m_p + 10 \div 20$ MeV. A constraint on small M_{pp} corresponds to the elimination of higher partial waves between the outgoing protons.

Fig. 13a shows the distribution of events as a function of $M_{pp\pi^-}$ with the constraint $M_{pp} < 2m_p + 18$ MeV. The solid curve corresponds to the phase space constrained by the same M_{pp} cut-off [4].

The data in Fig. 13a signal a bump at $M_{pp\pi^-} \approx 2.06$ GeV with a width ~ 15 MeV, which is of the order of the energy resolution of the set-up in this region of invariant masses.

In the $pp\pi^+$ mass spectrum, Fig. 13b, a similar structure is absent, and the observed spectrum is consistent with the phase space curve constrained by the set-up and by the M_{pp} cut-off.

The proton-proton invariant mass distribution from ITEP data is shown in Fig.18a. The solid curve presents Monte Carlo calculations for pure phase space. Constraints due to the experimental set-up were taken into account during simulations. The ratio of the experimental points (open squares on Fig.18a) to the corresponding values of pure phase space (the so-called correlation function) is shown on Fig.18b . One can observe the strong FSI effect at small M_{pp} values.

The proton-proton FSI affects the $p\pi^-$ invariant mass spectrum as may be seen in Fig.17b. It may also affect the $pp\pi^-$ invariant mass spectrum as well. To address this question, special Monte Carlo calculations were performed. The correction on the FSI effect was implemented into calculations. Numerically it was implemented exactly to satisfy experimental points on Fig.18a and b – see dashed curves on these figures. The only purpose of such an implementation was **not to study** the pp FSI itself but to find out **how it could affect** the $pp\pi^-$ invariant mass distribution.

The $pp\pi^-$ invariant mass distributions are shown on Fig.18c for all events and on Fig.18d for the events satisfying the $M_{pp} < 2m_p + 18$ MeV constraint. The solid curves on these figures are the Monte Carlo calculations for pure phase space. The ratio of the total number of the events to those with the $M_{pp} < 2m_p + 18$ MeV constraint in the framework of the pure phase space reaction mechanism is not a free parameter. Since this quantity is fixed and well-defined in the Monte Carlo calculations, one need normalize curves to the experimental data only once. The normalization was done for the total number of all events, Fig.18,c. IN ORDER TO DEFINITIVELY REMOVE the observed effect (experimental points vs solid curve on Fig.18d) the pure phase space curve was FORCED to be normalized to the total number of events in Fig.18d - dotted curve, and corrected to pp FSI - dashed curve. One can conclude that pp **FSI doesn't affect the shape of the** $pp\pi^-$ **invariant mass distribution** significantly and cannot fit observed experimental results

with reasonable ammount of accuracy even with ARTIFICIAL NORMALIZATION.

Electroproduction of the $pp\pi^-$ System off the ^3He .

If we confine our future investigation only to a deuterium target and if we find a narrow spike in the $pp\pi^-$ invariant mass distribution, then it would be extremely difficult to derive unambiguous conclusions about the nature of this effect. To illustrate this, consider two diagrams which could contribute in principle to the reaction mechanism - see Fig.19a and Fig.19b. We suppose here that the effect was produced in the $\pi-$ interaction with a very close pair of protons which could be considered as a single isolated individual object seen as (pp). Clearly, to distinguish between these two hypotheses one should either to utilize a number of model dependent assumptions and calculations, or perform detailed partial wave analysis of the data.

A tremendous improvement in our capacity to interpret the data would result if we were to extend our investigations to the lightest nuclei, such as ^3He and ^4He.

If the spike is a real resonance, then the quasifree machanism (see pole graph on Fig.20a) will provide the major part of the cross section. The cross section in this case should be close to the same value for the deuterium target, and what seems much more important,, we should observe a well defined and apriori predicted (flat?) Treiman-Yang distribution. The Treiman-Yang criterion is absolutely model independent and is the clearest direct indication of any quasi-free reaction.

If, however, the spike is provided by the strong final state interaction in the $pp\pi^-$ system, then in addition to the quasi-free mechanism of Fig. 20b we should expect a significantly larger value of the cross section compared to a deuterium target due to another channel of the reaction with quasi-free π^- production off neutron and its subsequent rescattering on the closely correlated pair of two protons, see Fig. 20c. The Treiman-Yang criterion should fail in this case. This would be the strongest and most unspeculative evidence in favour of the FSI nature of the observed effect.

Alternative d' searches. The Pionic Double Charge Exchange Reaction (DCX)

As a result of common efforts undertaken at LAMPF, TRIUMF, and PSI there now exists a substantial base of low-energy DCX data on light and medium nuclei, which all exhibit a very regular and smooth angular dependence at higher energies – as predicted by various theoretical models – however, they also exhibit a peculiar and totally unexpected energy behaviour near $T_\pi \approx 50$ MeV [5]. This feature has been seen for both double isobaric analog transitions (DIAT) and for ground state transitions (GST).

As shown recently, this puzzling energy behaviour, which as of yet has not been understood within current models, finds its natural explanation by the narrow d' resonance. Fig. 14 shows the most recent results on the DCX reaction $\pi^+ \, ^{40}Ca \rightarrow ^{40} Ti \, \pi^-$ obtained at PSI. The solid curve represents theoretical predictions based on the d' hypothesis.

The parameters of the d' for mass and width, $M_{d'} \approx 2.06$ GeV, $\Gamma_{NN\pi} \approx 0.5$ MeV, deduced from DCX–data, characterize the d' resonance embedded in nuclear medium.

To rule out nuclear medium effects in the DCX reaction one ideally would need measurements on a dineutron or diproton which are unbound. The next best choice for DCX

would be ^{3}He and ^{4}He, where medium effects are expected to be strongly reduced or absent. The presently available data on low energy DCX on ^{4}He, where conventional reaction mechanisms are heavily suppressed by the Pauli exclusion principle, agree very favorably with the predictions based on the d'-hypothesis. In the latter reaction, the d' is expected to manifest itself as a threshold phenomenon at $T_\pi \sim 80 - 100$ MeV.

References

1. J.M. Laget. *Nucl. Phys.*, **A358**, 275c, 1981.
2. H. Arenhövel. *Phys. Lett.B*, **199**, 13, 1987.
3. P.J. Mulders, A.T. Aerts, J.J. de Swart. *Phys. Rev.*, **D21**, 2653, 1980
   L. Kondratyuk, B. Martemyanov, M. Schepkin. *Yadern. Fiz.*, **45**, 1252, 1987.
4. L. Vorobyev et al. *JETP Lett.*, **59**, (No.2), 1994.
5. R. Bilger, H. Clement, M. Schepkin. *Phys.Rev.Lett.*, **47**, 42, 1993.
   R. Bilger et al. *Z. Phys.*, **A343**, 491, 1992.
   H. Clement, et al. *Nucl. Phys.*, **A553**, 589c, 1993.
   B. Martemyanov, M. Schepkin. *JETP Lett.*, **53**, 139, 1991.
   H. Clement, M. Schepkin, G.J. Wagner, O. Zaboronsky. *Phys. Lett.B*, **337**, 43, 1994.
6. L.D. Blokhintsev et al. *Sov. Phys. JETP*, **15**, 1136, 1962.
   E.I. Dubovoi and I.S. Shapiro, *Sov. Phys. JETP*, **24**, 839, 1967.
   O.D. Dalkarov and V.M. Kolybasov, *Sov.J.Nucl.Phys.*, **18**, 416, 1974.
   V.M. Kolybasov. Moving triangle singularities : the possibilities for observation in deuteron reactions. Report on Intern. Symposium "Dubna Deuteron-95". Proc. of the Symposium, in print.
7. Deuteron Electrodisintegration at Threshold at large momentum transfers. E–89–047
8. Electroexcitation of the $\Delta(1232)$ in Nuclei. E–89–017.
9. Measurement of the $\Delta - \Delta$ Component of the Deuteron by Exclusive Quasielastic Electron Scattering. E–93–043.
10. S. Stein et al. *Phys. Rev.*, **D12**, 1884, 1975.
11. W. Bartel et al. *Phys. Lett.B*, **28**, 148, 1968.
12. M. Lacombe et al. *Phys. Lett.B*, **101**, 139, 1981.
13. R.J. Loucks, V.R. Pandharipande, R. Schiavilla. *Phys. Rev.* **C49**, 342, 1994
14. A.P. Kobushkin. *Sov.J.Nucl.Phys.*, **28**, 495, 1978.
15. see, e.g., T. Ericson and W. Weise: Pions and Nuclei, Clarendon Press, Oxford.
16. V.M. Kolybasov. Yad. Fiz. (Soviet J.Nucl.Phys.) 25(1977)209.
17. K.K. Seth. Int. Conf. on Medium and High Energy Physics, Taipei, Taiwan, 1988.
    E.N. Komarov. Preprint 1853. Petersburg Nucl. Phys. Inst., 1993.
18. M. Schepkin, O. Zaboronsky, H. Clement. *Z. Phys.*, **A345**, 407, 1993.
19. R. Bilger e.a. *Nucl. Phys. A*, 1996. To be published.
20. Particle Data Group. *Review of Particle Properties. Phys. Rev.*, **D50**, No.3, 1994.

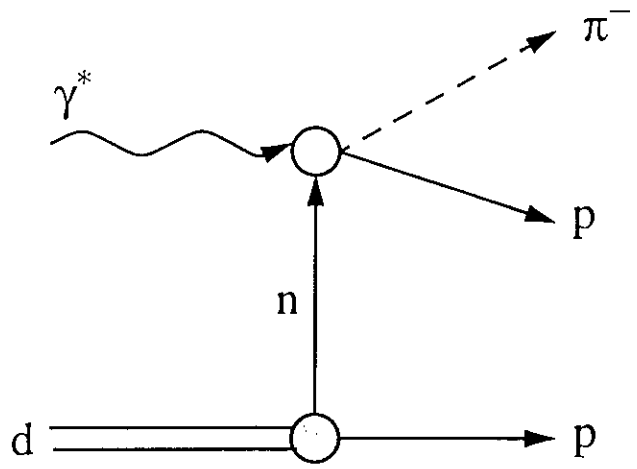

a)

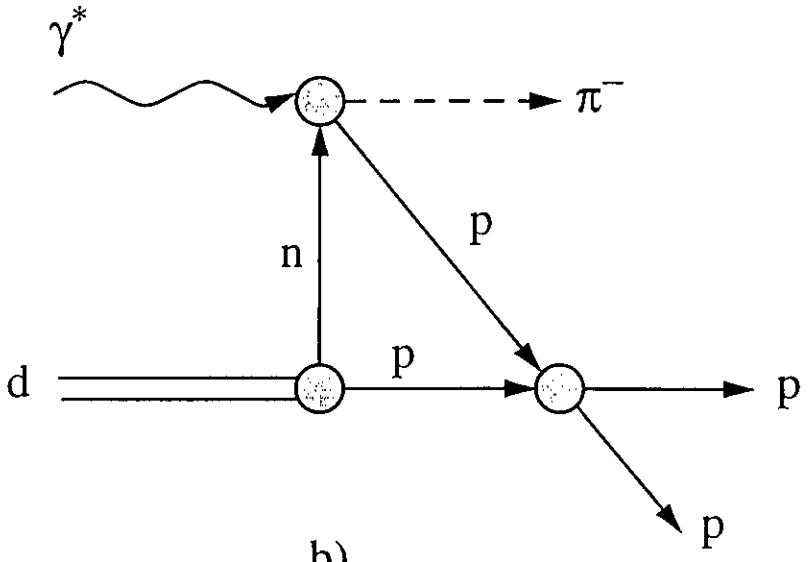

b)

Fig. 1.

Pole (a) and triangle (b) graph with *pp*-rescattering.

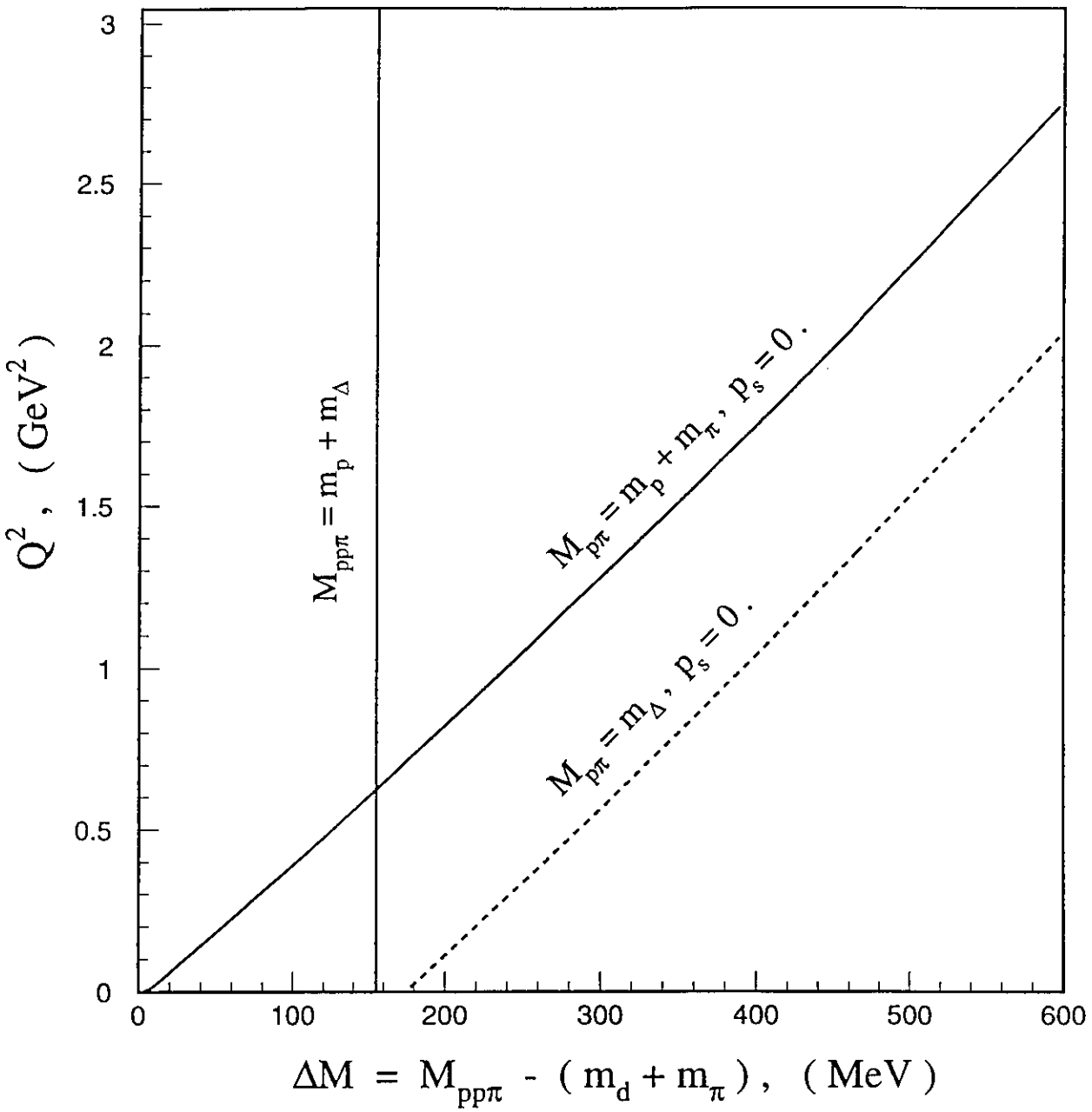

Fig. 2. Kinematics for $pp\pi^-$-production on deuterium target. Inclined curves correspond to the quasifree mechanism (nucleon-spectator at rest). Vertical lines correspond to the interection with the deuteron as a whole.

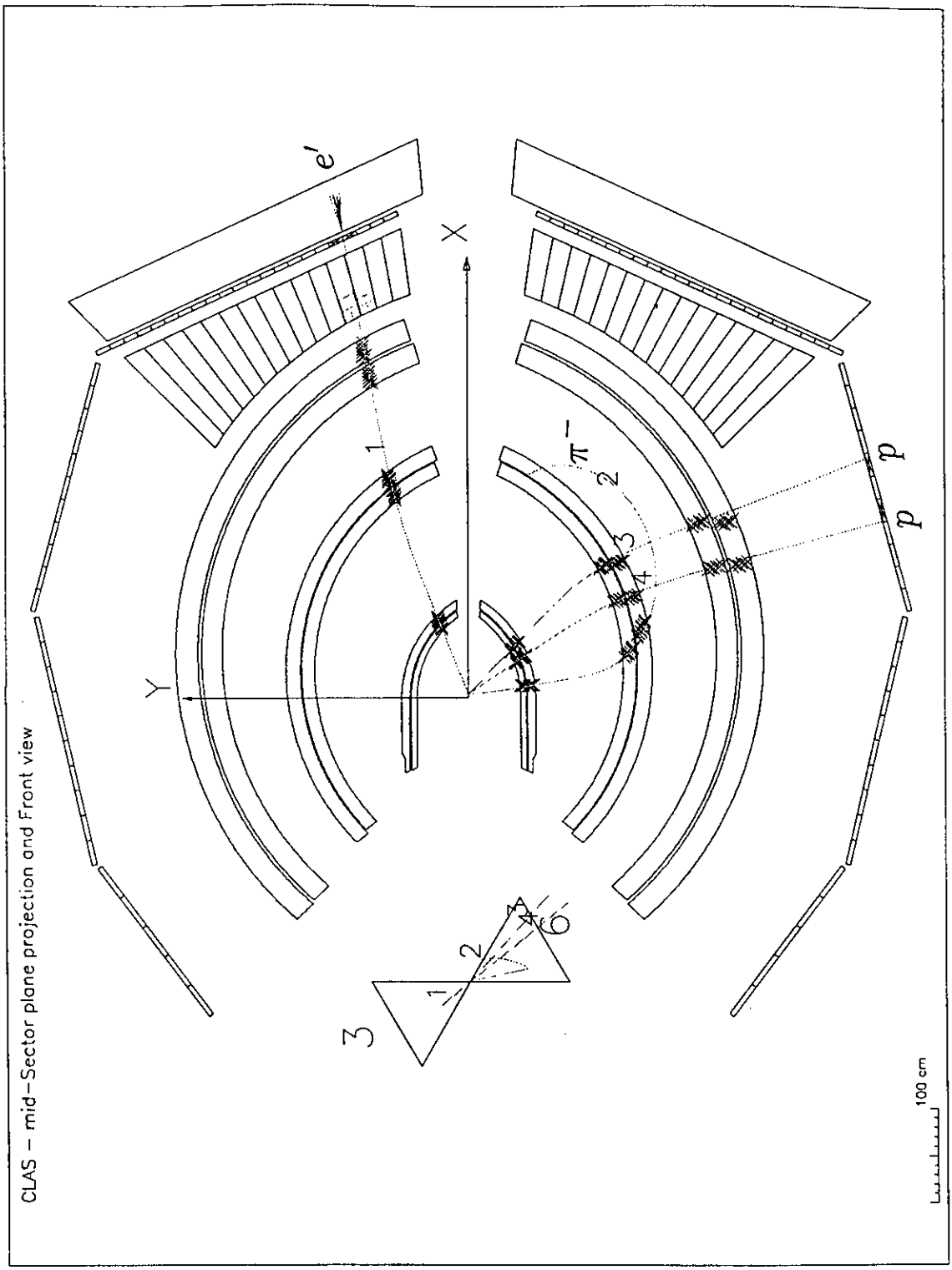

Fig.3. Typical event at $\Delta M < 100$ MeV.

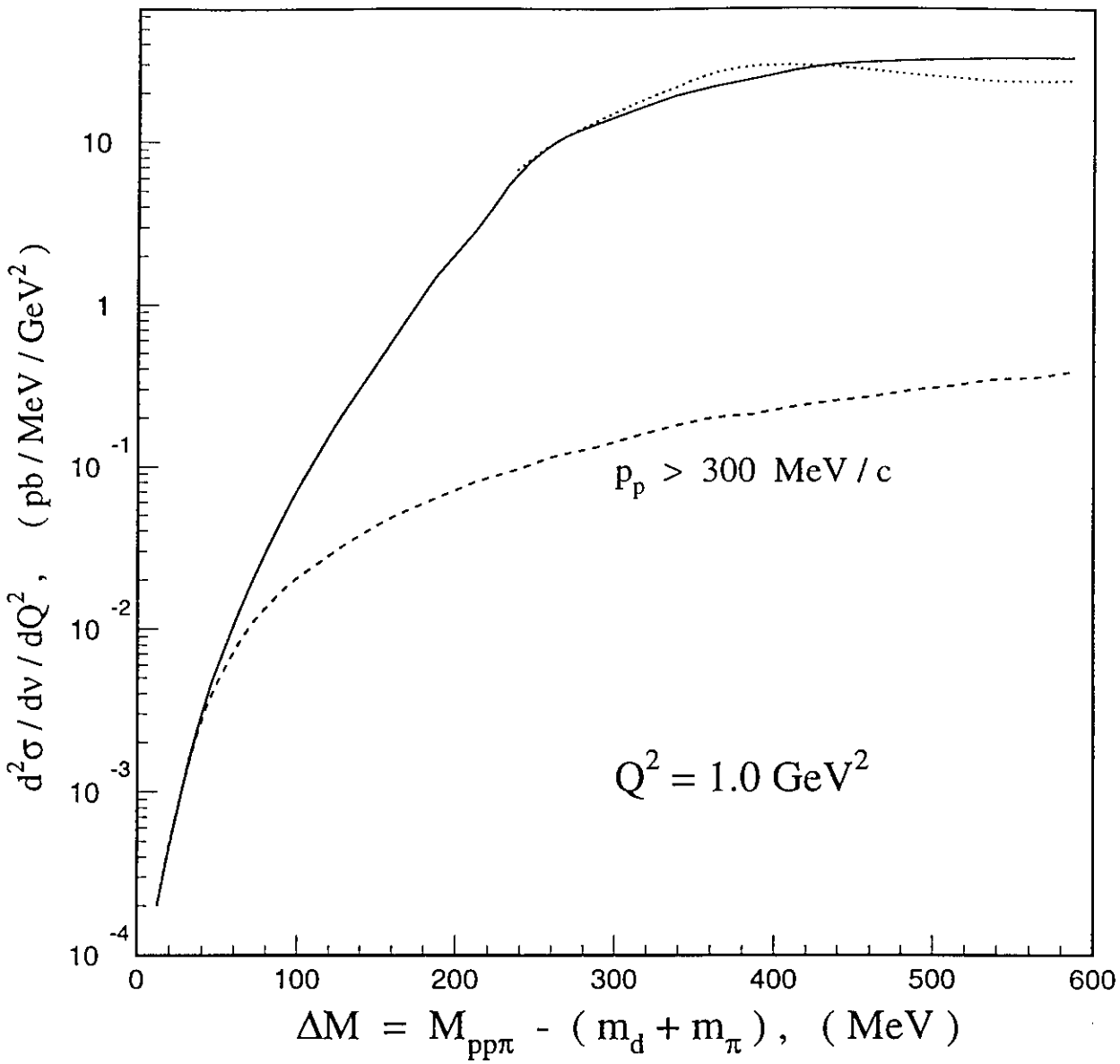

Fig. 4,a. Cross section as a function of ΔM. Dots - experimental data [10] divided by factor 3, which corresponds to the ed $\rightarrow$ eppπ^- channel. Solid curve - calculations in the frame work of quasifree mechanism with Paris deuteron wave function [12] normalized to experimental data (dots). Dashed curves - the same as soloid except for the constraint of protons momenta $p_p > 300$ MeV/c.

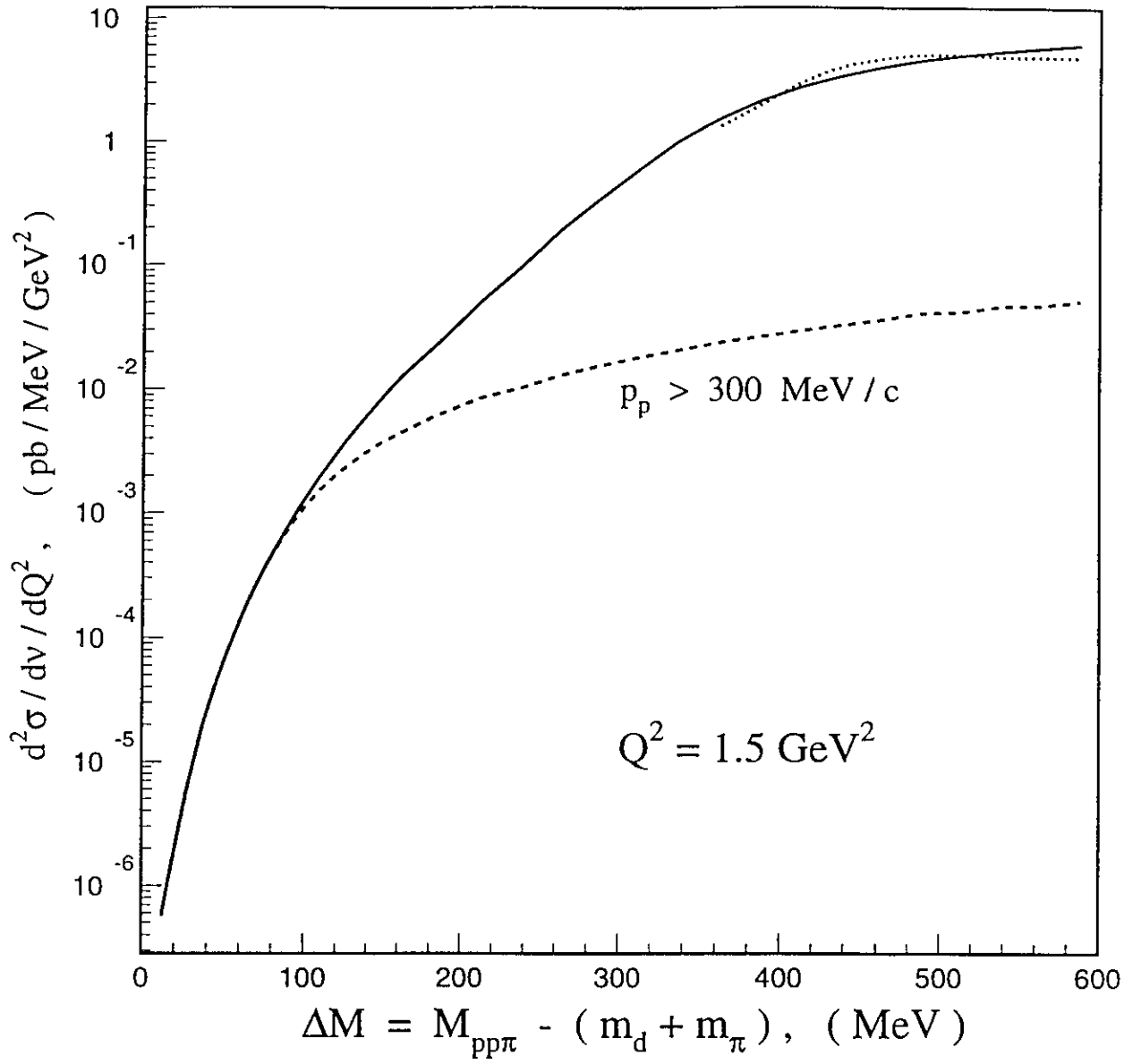

Fig. 4,b. The same as on Fig.4,a but for $Q^2 = 1.5\ GeV^2$.

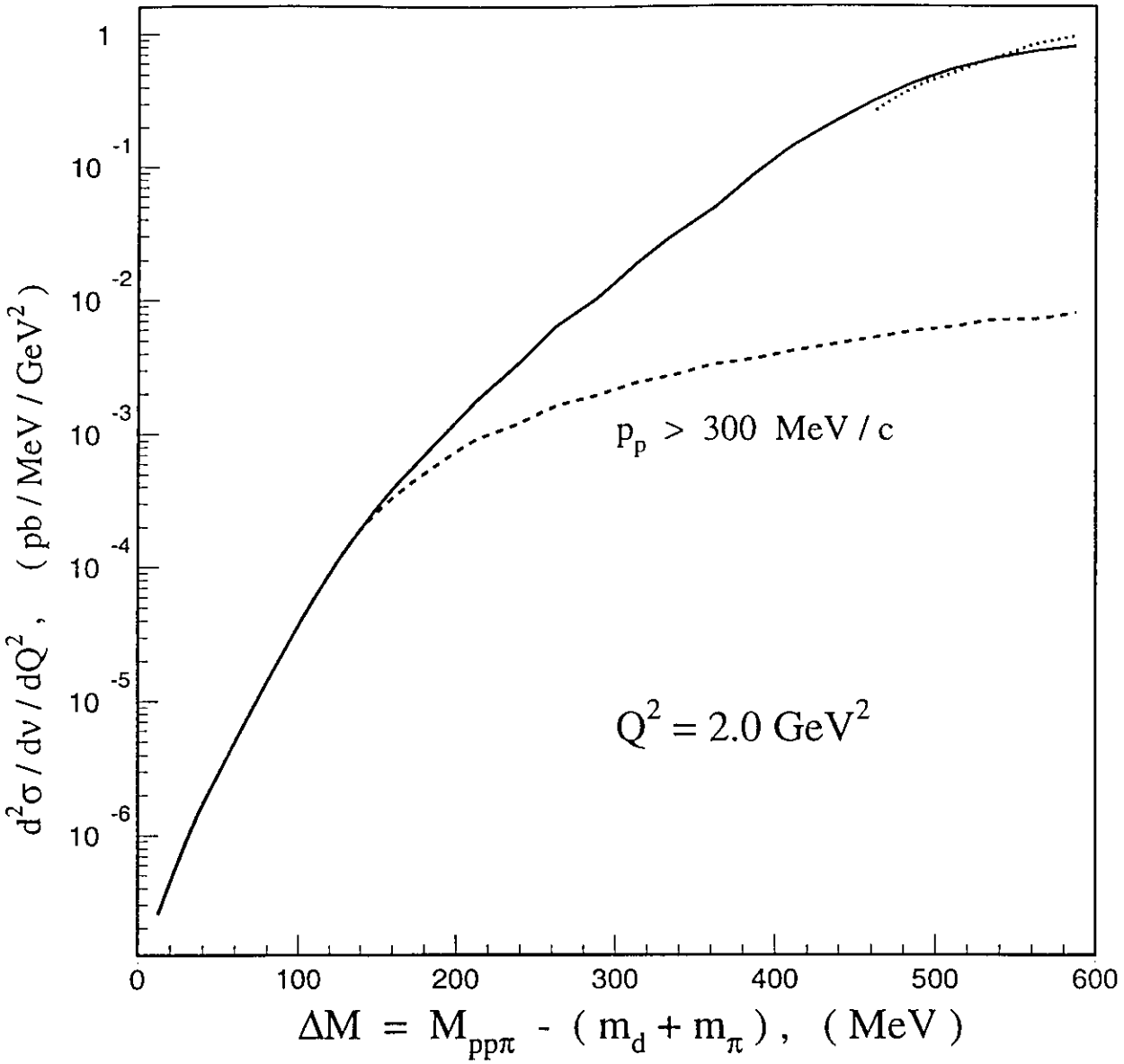

Fig. 4,c. The same as on Fig.4,a but for $Q^2 = 2.0$ GeV^2.

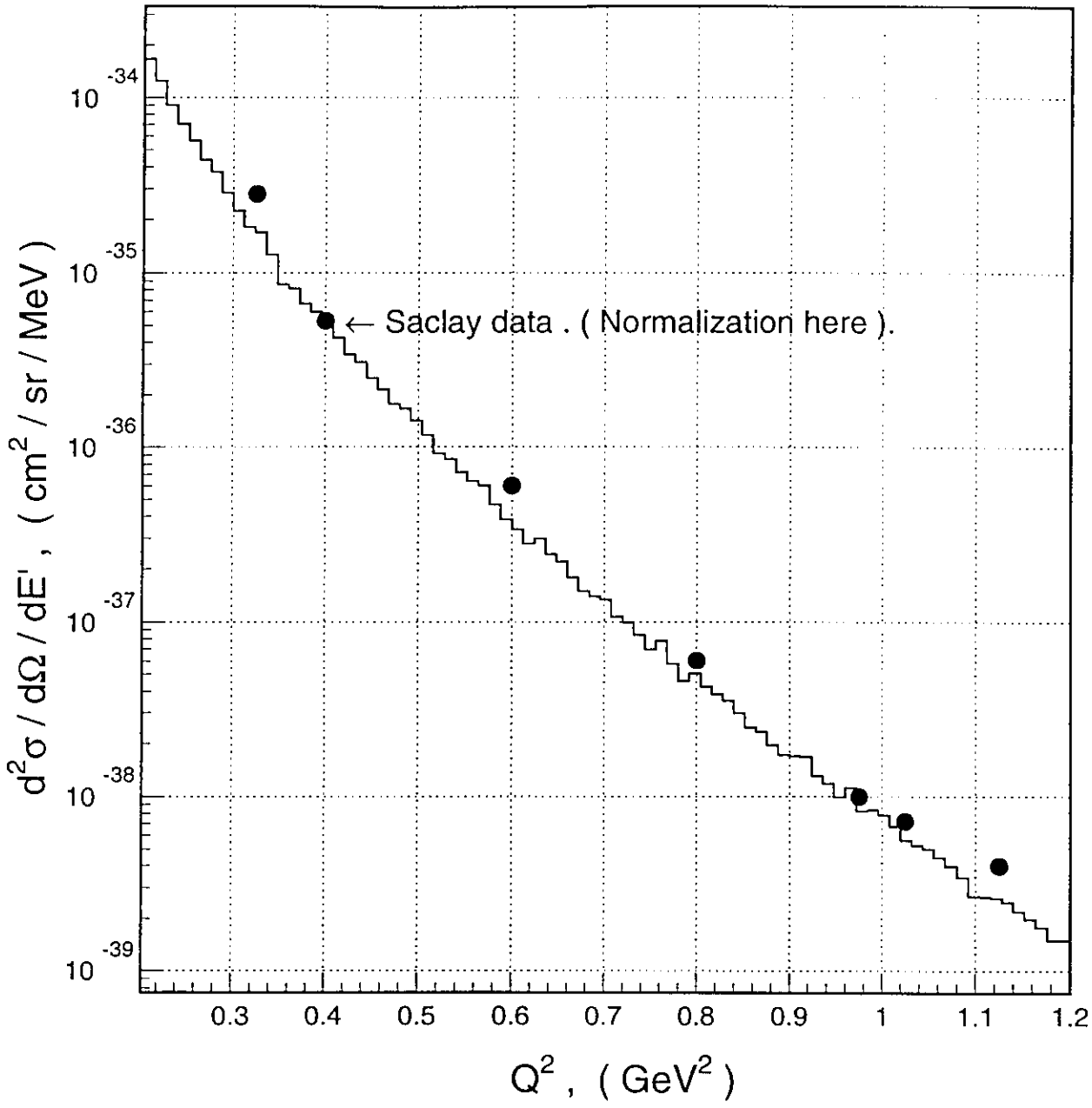

Fig. 5. Comparison of Q^2-dependence of the cross section for the quasifree mechanism at $\Delta M < 25$ MeV with Q^2-dependence of the deuteron desintegration near threshold [15] .

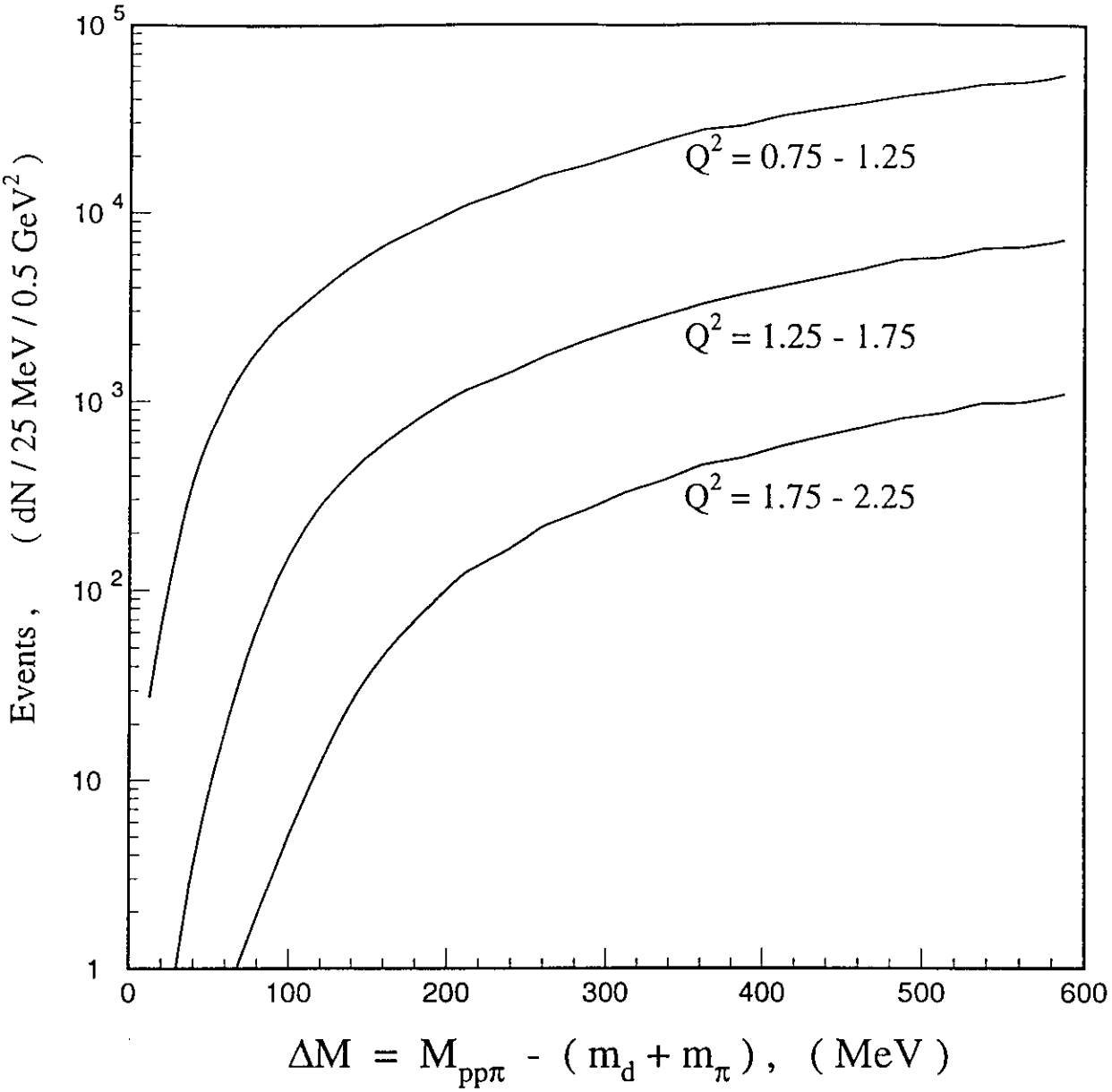

Fig. 6. The expected statistics per $M_{pp\pi}$ invariant mass interval 25 MeV and for three intervals of Q^2 : 0.75 - 1.25 , 1.25 - 1.75 , 1.75 - 2.25 GeV^2.

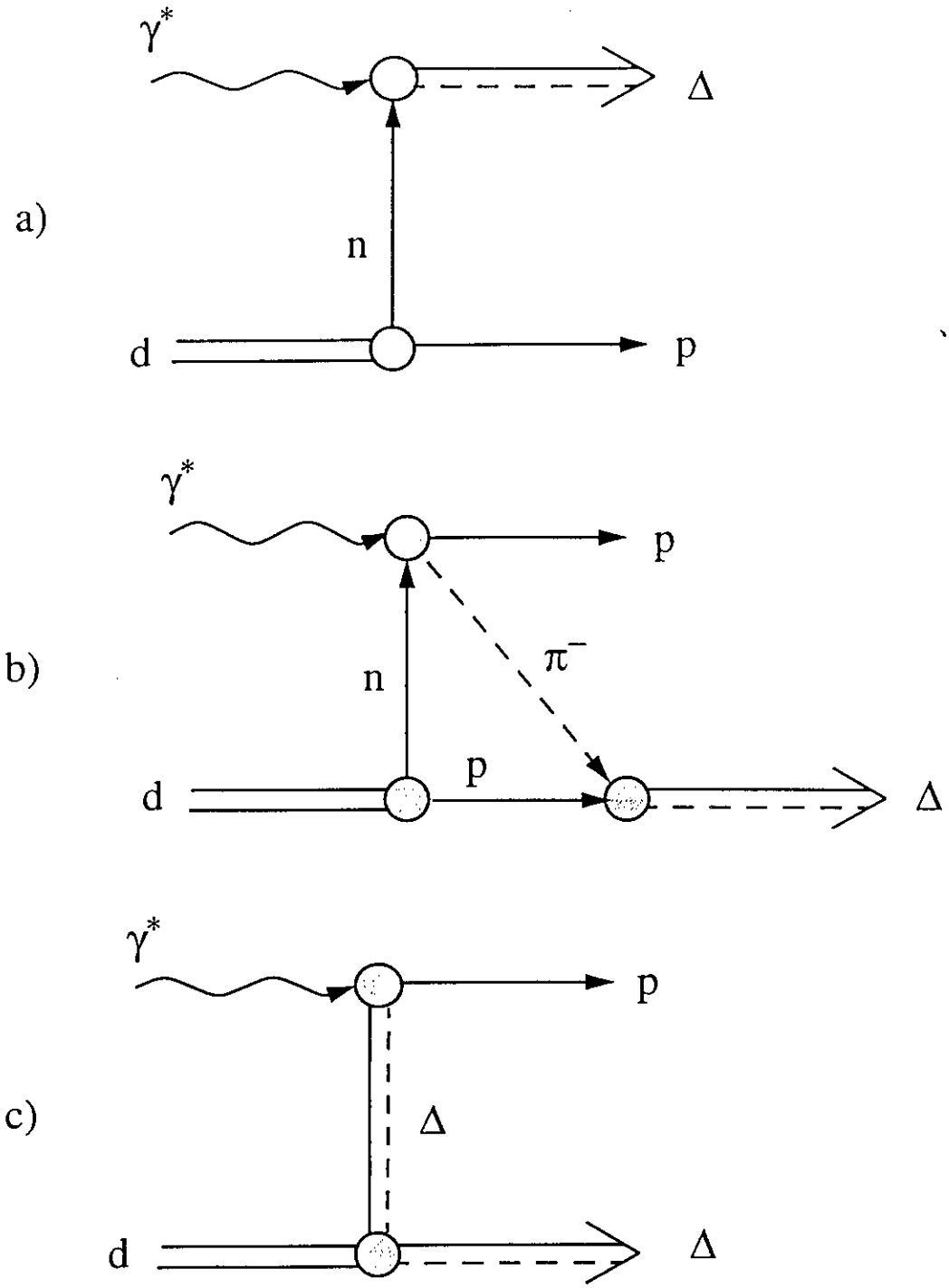

Fig. 7

Graphs with Δ–isobar production in the final state.

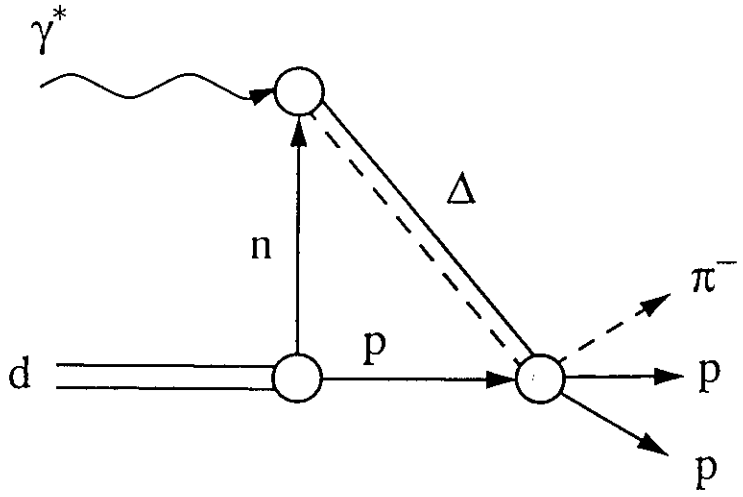

a)

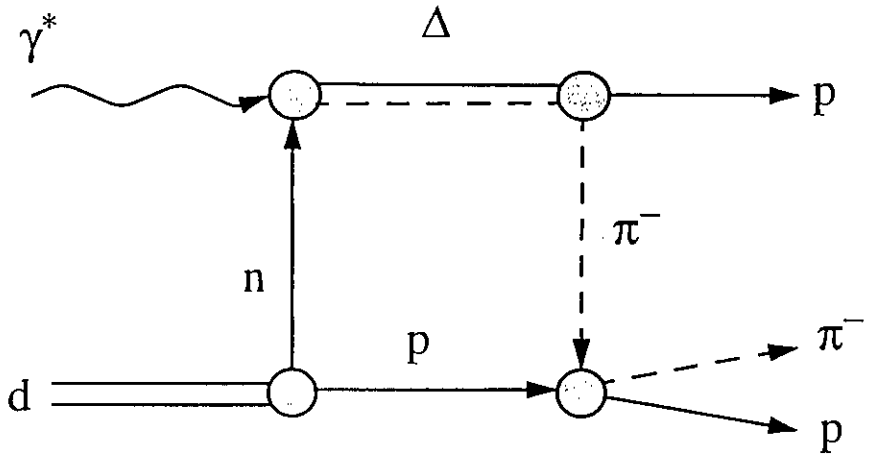

b)

Fig. 8

Graphs with Δ-isobar in the intermidiate state.

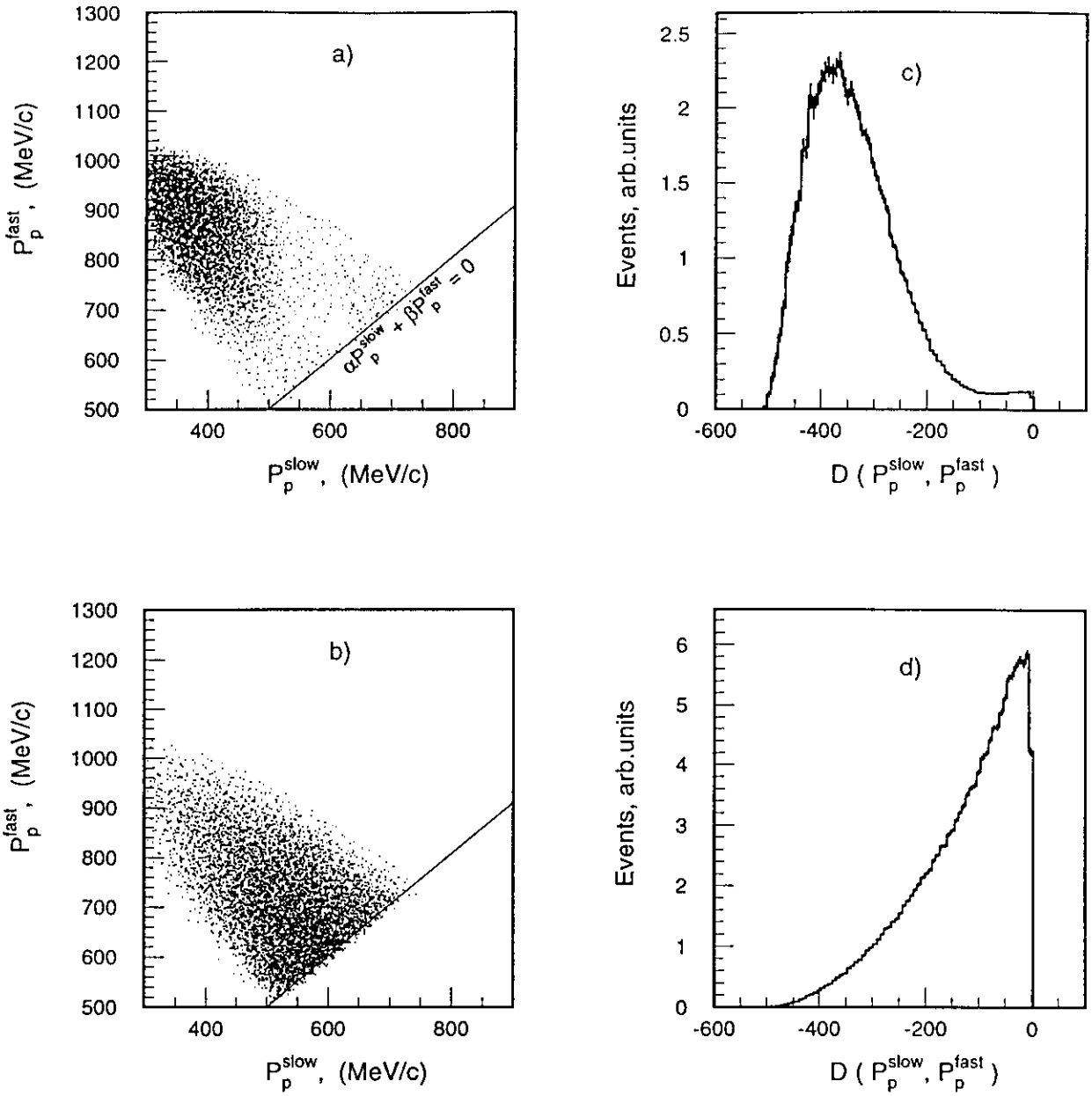

Fig. 9. $Q^2 = 1.5\ GeV^2$, $\Delta M_{pp\pi} < 100$ MeV.

Two dimensiopnal plots. Horisontal axis - momentum of the "slow" proton.
Vertical axis - momentum of the "fast" proton. "D" is defined as a linear combination :
$D = \alpha P_p^{slow} + \beta P_p^{fast}$. a) and c) - pole graph, b) and d) - triangle graph.

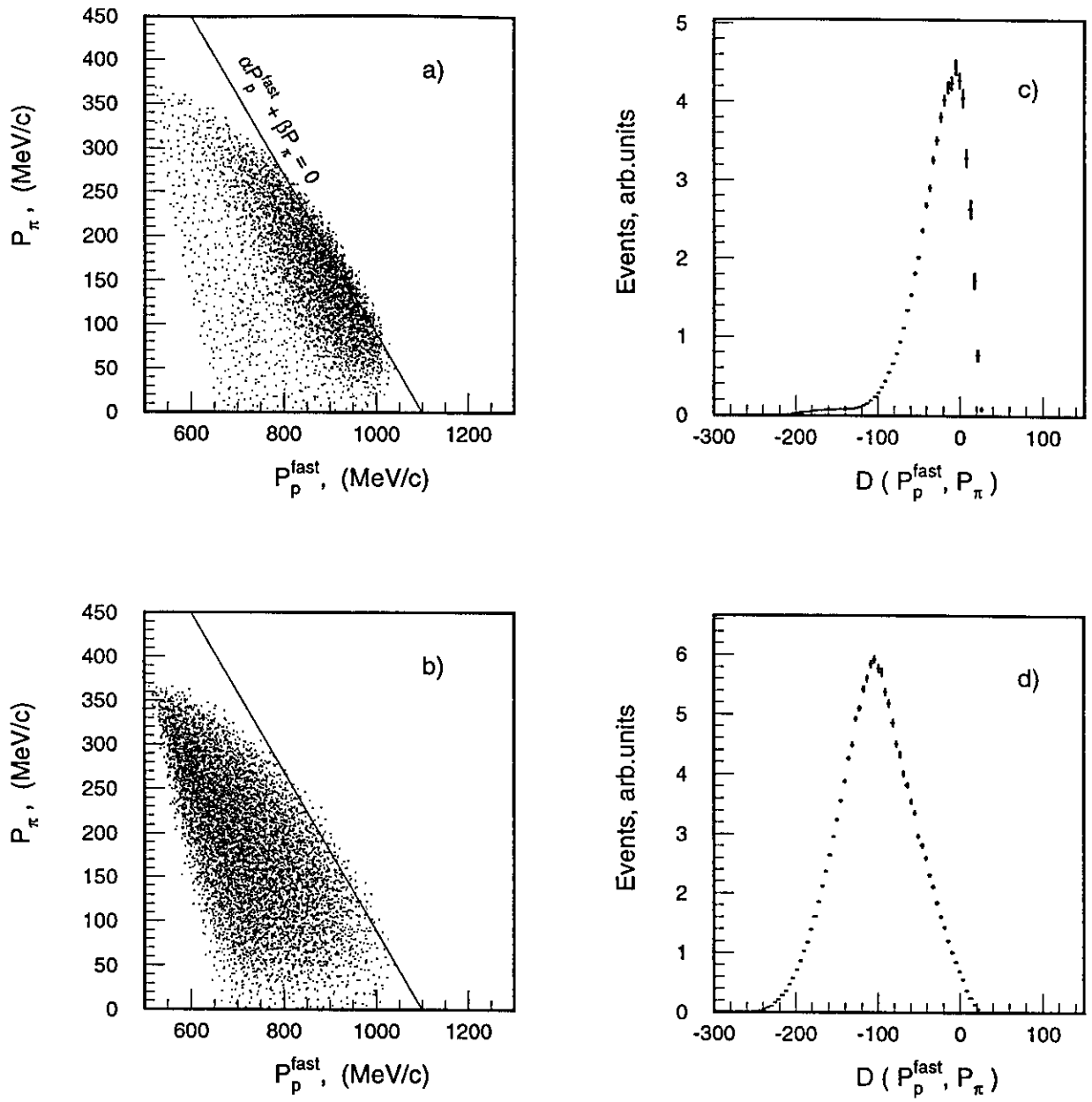

Fig. 10. $Q^2 = 1.5\ GeV^2$, $\Delta M_{pp\pi} < 100$ MeV.

Two dimensional plots. Horisontal axis - momentum of the "fast" proton.
Vertical axis - pion momentum. "D" is defined as a linear combination : $D = \alpha P_p^{fast} + \beta P_\pi$.
a) and c) - pole graph, b) and d) - triangle graph.

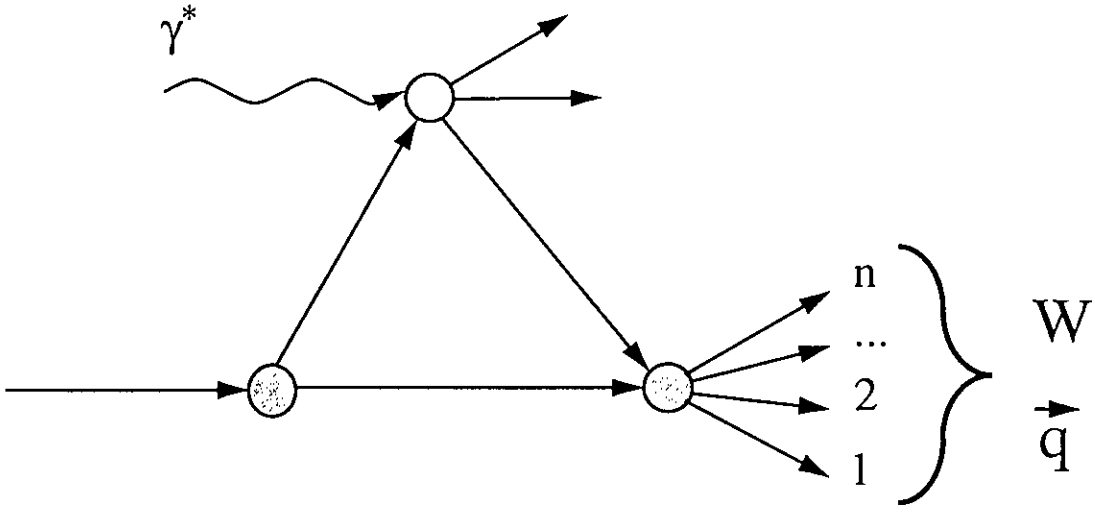

Fig. 11

The triangle graph.

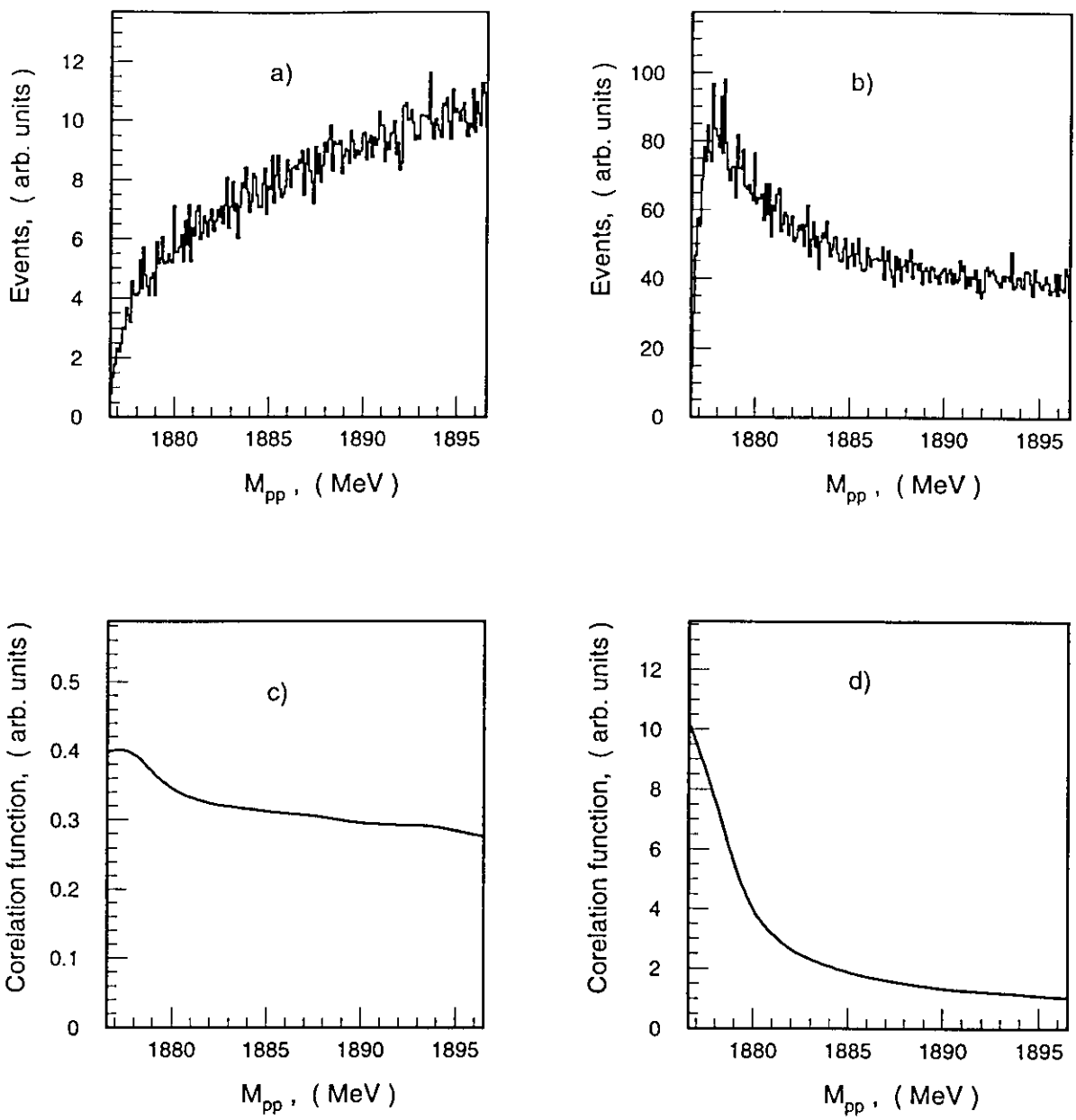

Fig. 12. a) - M_{pp} invarint mass distribution for the pole graph (fig.5,a)
b) - M_{pp} invarint mass distribution for the triangle graph (fig.5,b)
c) and d) - corelations functions, obtained by deviding distributions in (a) and (b), respectively, by M_{pp} phase space distribution.

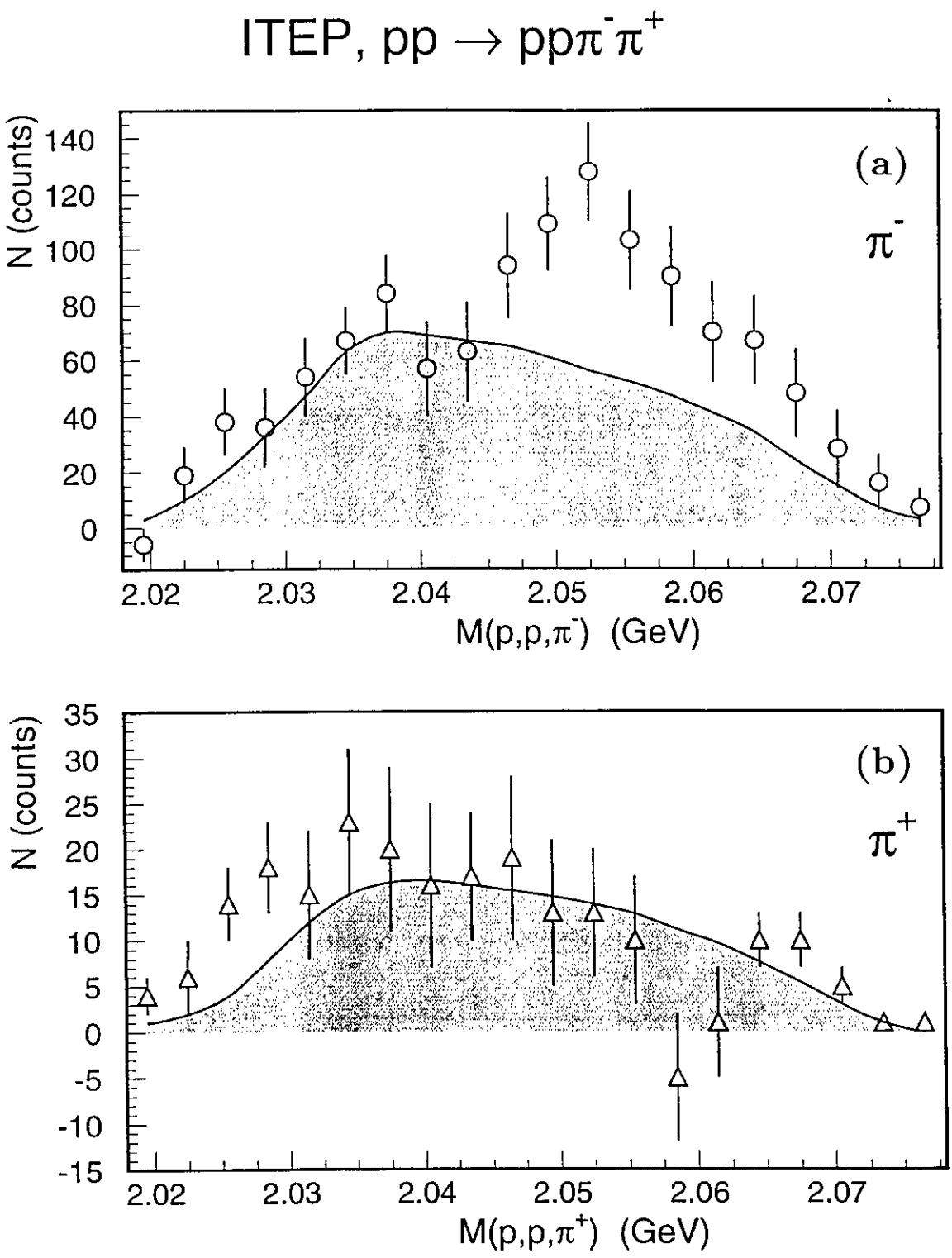

Fig.13. $pp\pi^-$ (a) and $pp\pi^+$ (b) invariant mass distributions in the reaction $pp \to pp\pi^-\pi^+$ with the constraint $M_{pp} < 2m_p + 18$ MeV [4].

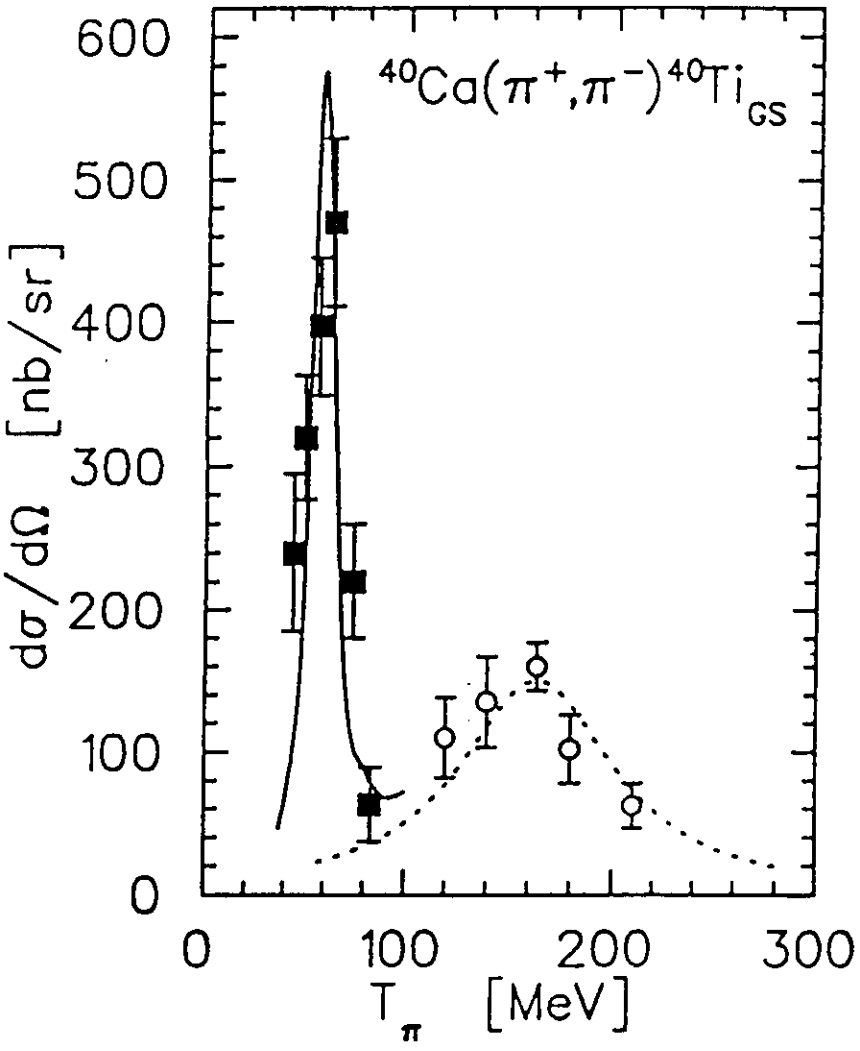

Fig.14. Recent experimental results on the pionic double charge exchange (To be published).

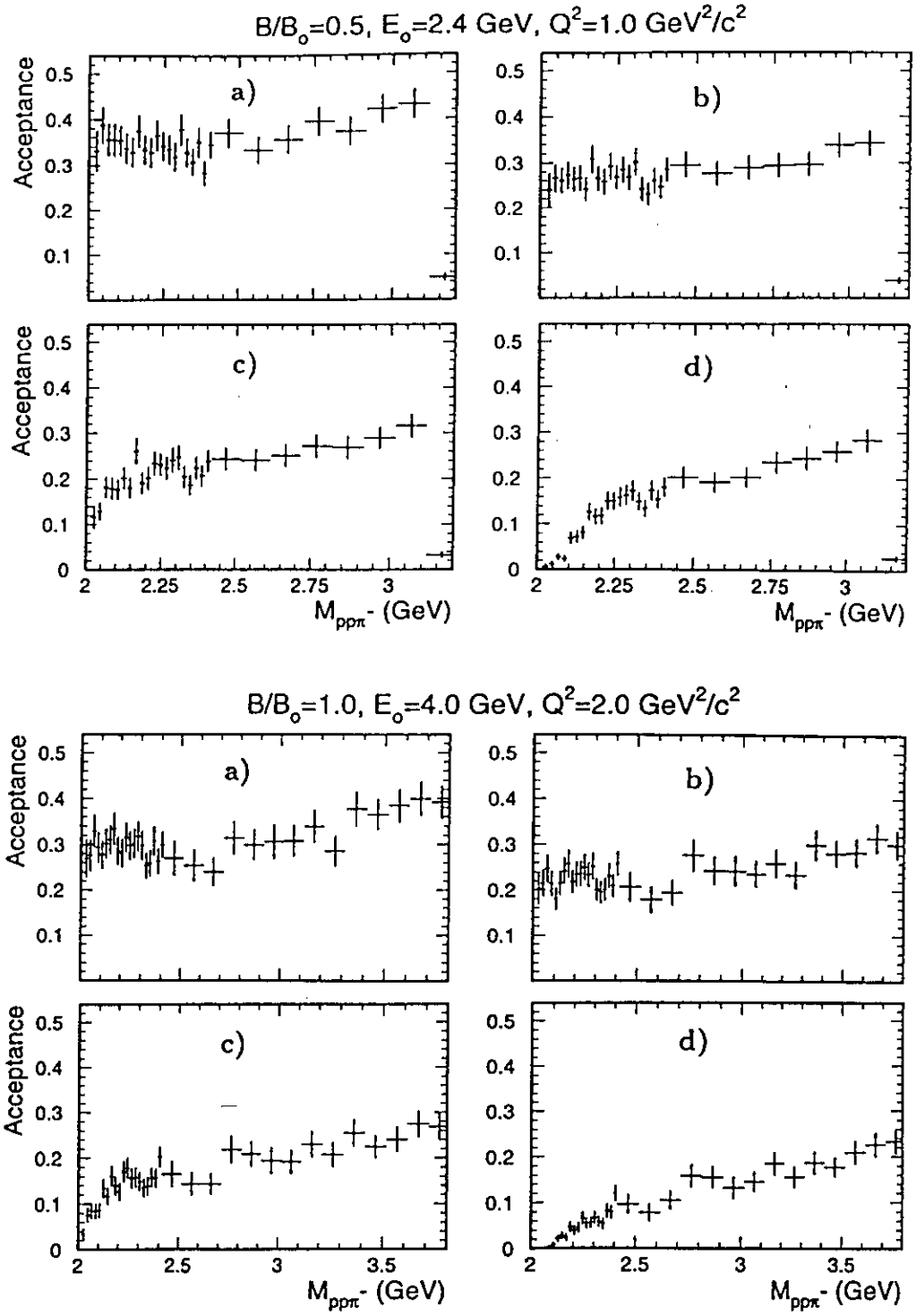

FIG.15

CLAS acceptance as a function of $pp\pi^-$ invariant mass for different sets of Magnetic Field (B/B_o), Electron Energy E_o, and 4-momentum transfere squared Q^2. Different "triggers" are considered :

a) only e' and two protons with so called "good tracks" (hits in all DC regions, and hits in TOF counters) are detected and reconstructed;

b) same as a), and with π^- hits in DC region 1;

c) same as b), and with π^- hits in DC region 2;

d) same as a), and with good track for π^-.

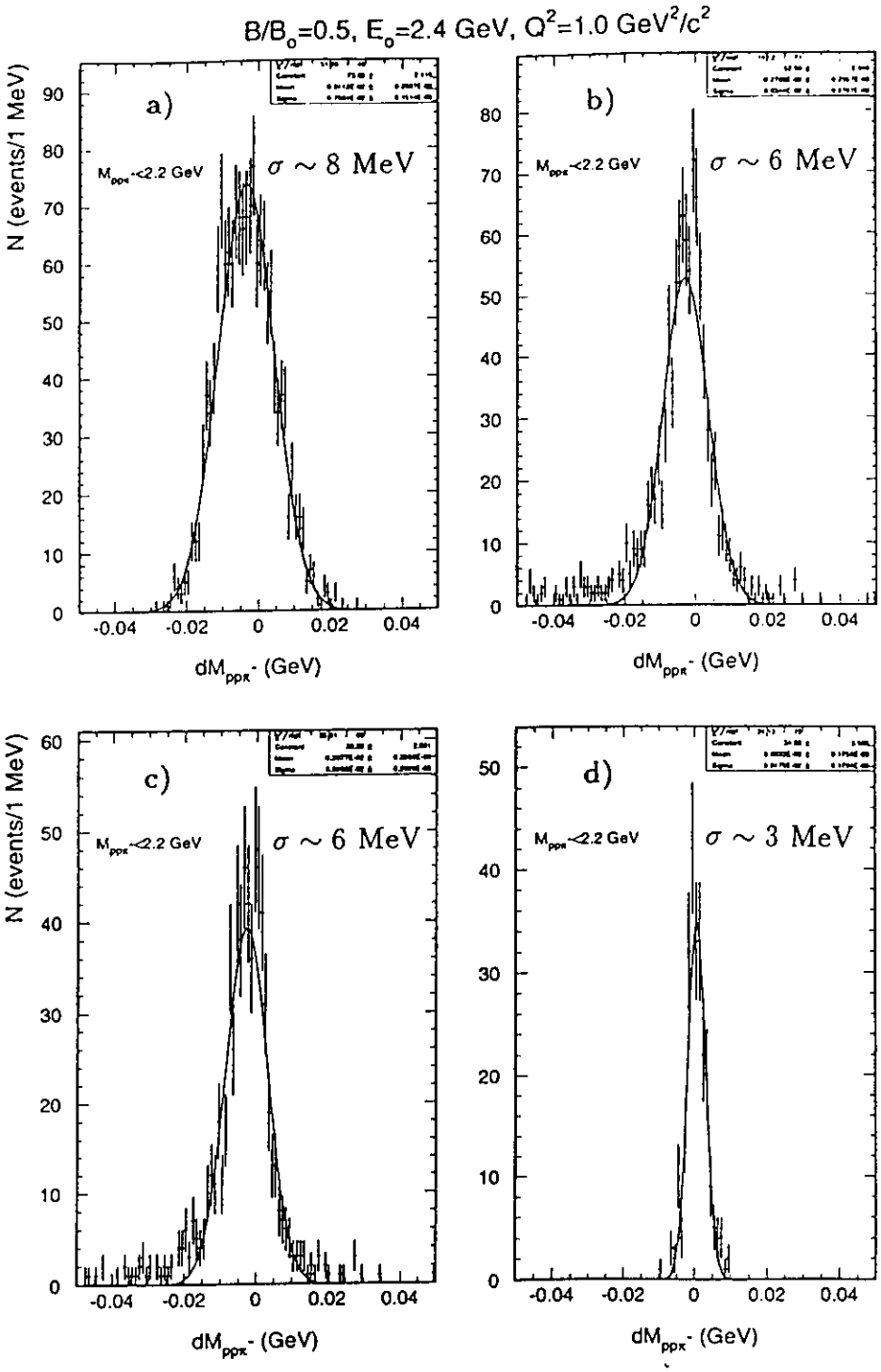

FIG.16

CLAS resolution in the $pp\pi^-$ invariant mass for $2m_p + m_{\pi^-} < M_{pp\pi^-} < 2.2\ GeV$ and for different sets of Magnetic Field (B/B_o), Electron Energy E_o, and 4-momentum transfere squared Q^2. Different "triggers" are considered :

a) only e' and two protons with so called "good tracks" (hits in all DC regions, and hits in TOF counters) are detected and reconstructed;
b) same as a), and with π^- hits in DC region 1;
c) same as b), and with π^- hits in DC region 2;
d) same as a), and with good track for π^-.

pp Final State Interaction and Pure Phase Space.

pp and $p\pi^-$ Invariant Mass Distributiions.

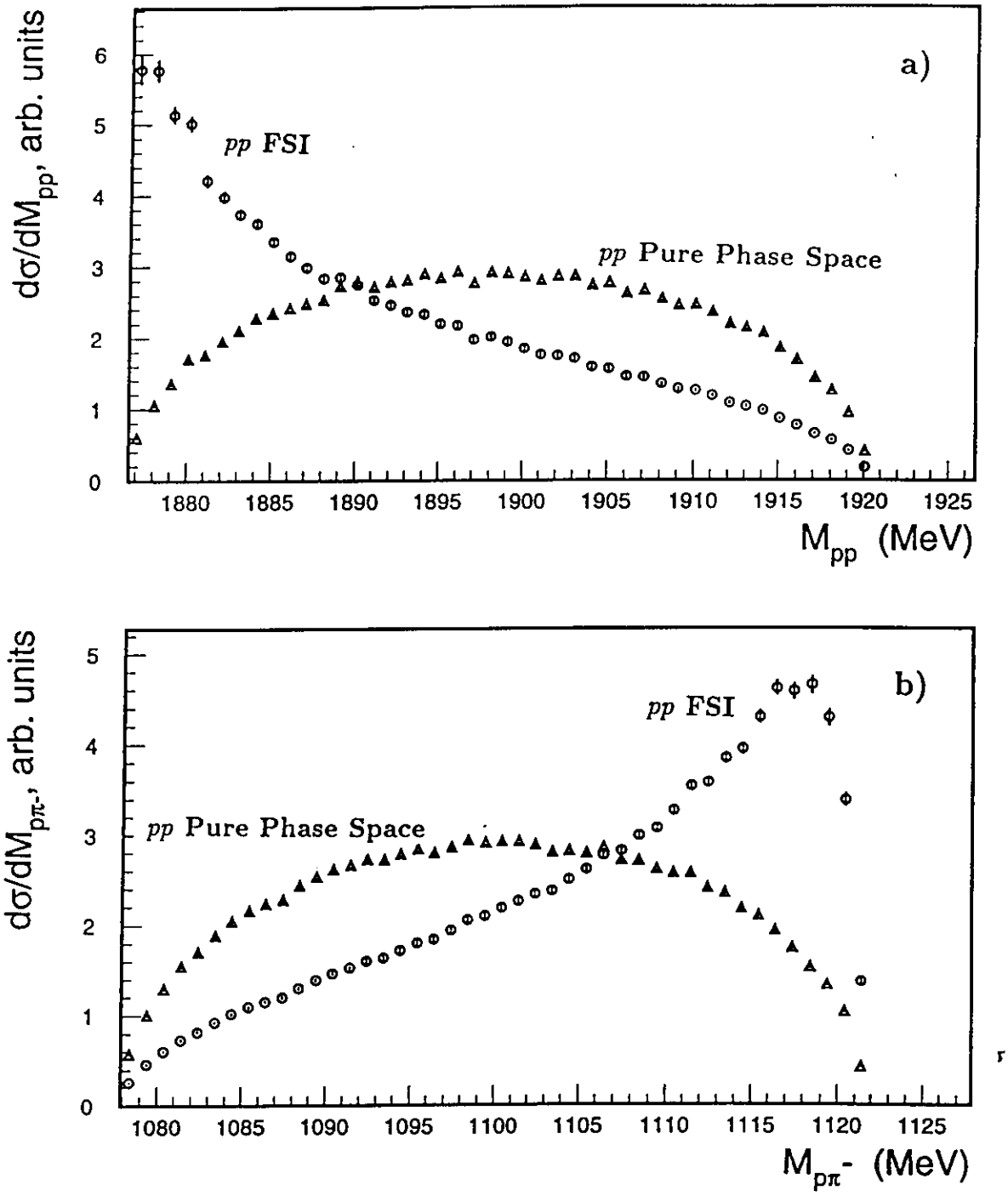

FIG.17

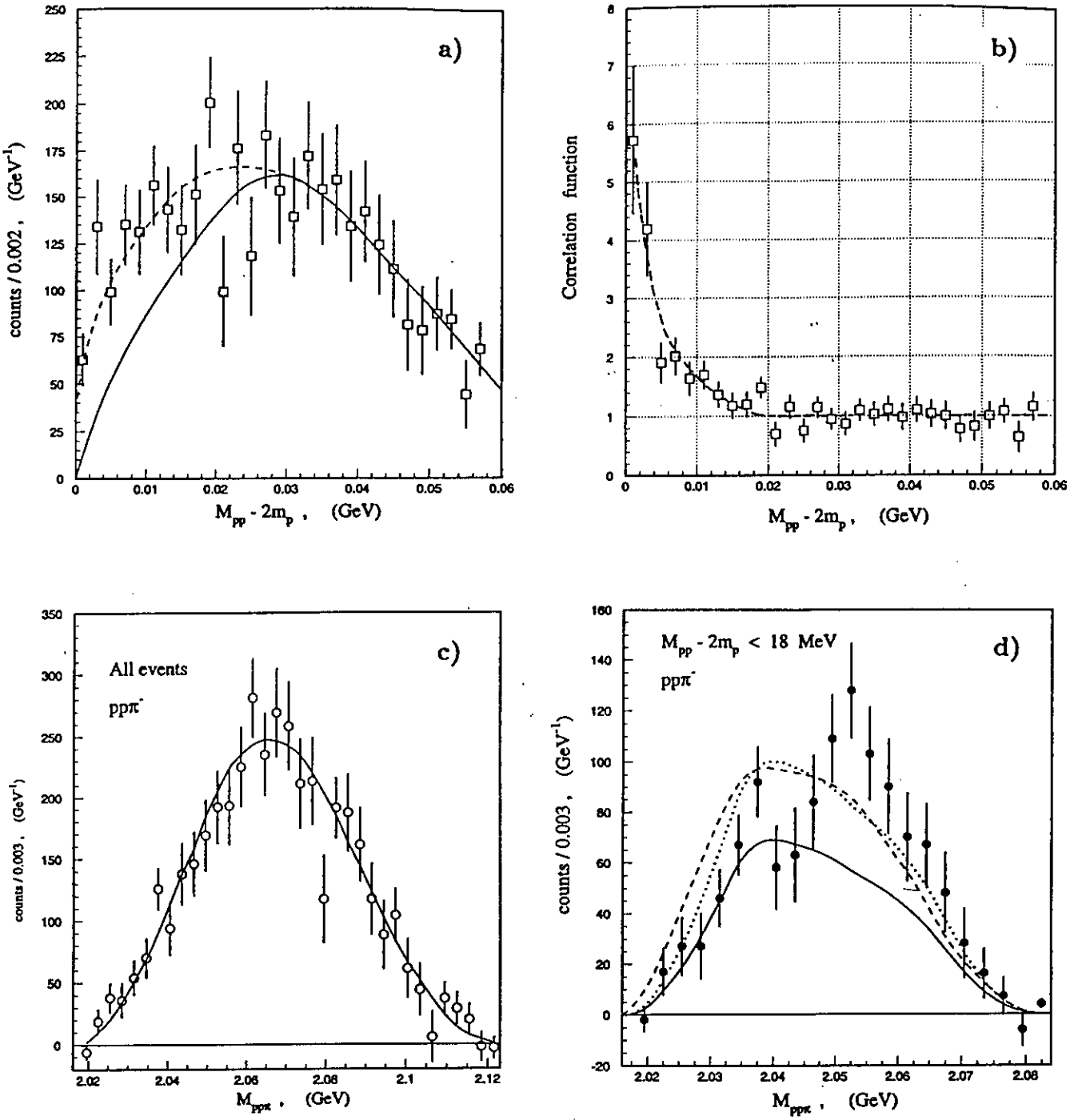

FIG.18

Two and Three Body Invariant Mass Distributions.
$pp \to pp\pi^-\pi^+$ ITEP Data, [4].

a) Proton-proton invarinat mass distribution. Solid curve - MC calculations for the pure Phase Space. Dashed curve - Phase Space + FSI .

b) Proton-proton correlation function.

c) The $pp\pi^-$ invariant mass distribution. Solid curve - MC calculations for the pure Phase Space.

d) The $pp\pi^-$ invariant mass distribution with the constrain on M_{pp}. Solid curve - MC calculations for the pure Phase Space. Dotted curve - the same as solid, but with normalization to the total number of events in this plot. Dashed curve - 'dotted' + FSI (see dashed curve on the Fig,a)).

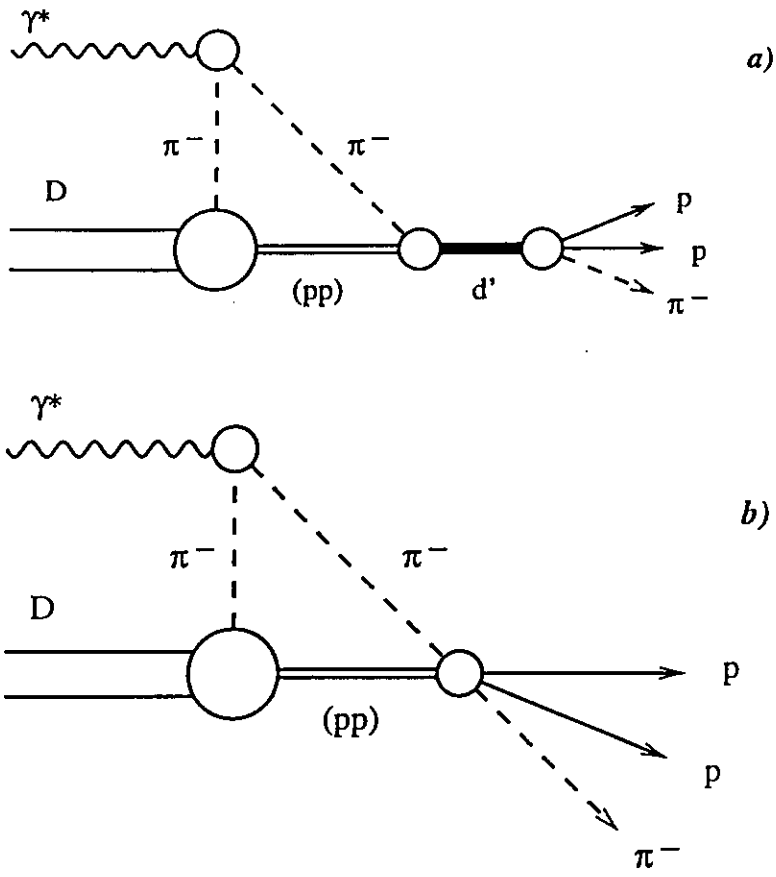

FIG.19

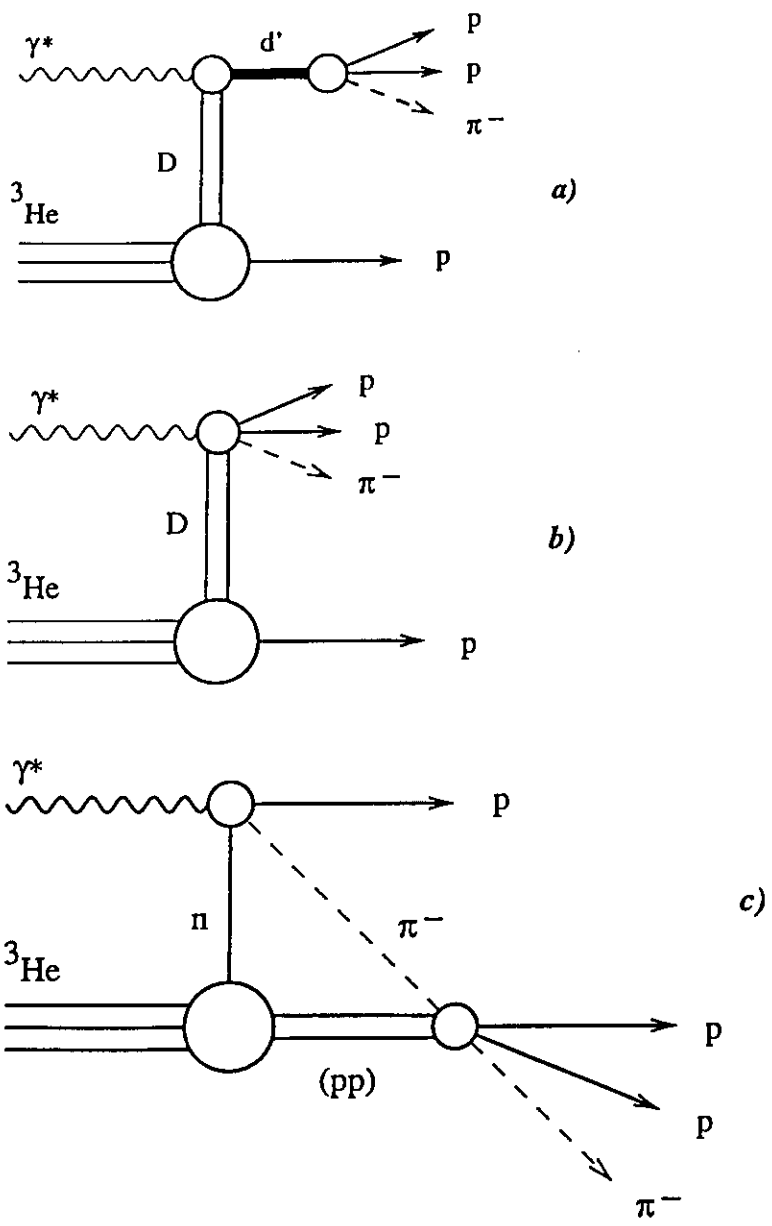

FIG.20